5. PHYSICAL OCEANOGRAPHY AND ASSOCIATED TASKS DURING MOSAIC LEG 1

Ying-Chih Fang[1], Mario Hoppmann[1], Hailun He[2]
Musheng Lan[3], Rainer Graupner[1]

(not on board) Benjamin Rabe[1], Sandra Tippenhauer[1], Markus Janout[1], Ilker Fer[4], Arild Sundfjord[5], Celine Heuze[6], Monika Rhein[7], Christian Mertens[7], Yusuke Kawaguchi[8]

[1]DE.AWI
[2]CN.SIO
[3]CN.PRIC
[4]NO.UIB
[5]NO.NPOLAR
[6]SE.GU
[7]DE.UNI-Bremen
[8]JP.AC.U-TOKYO

Grant-No. AWI_PS122_00

A comprehensive summary of the physical-oceanographic measurements during all 5 cruise legs can be found in Rabe et al., 2022.

Background and Objectives

1. General physical oceanography of the central Arctic Ocean

The thinning of the Arctic sea ice in the Eurasian Basin makes the ocean underneath the ice more prone to be influenced by the atmospheric forcing. This scenario causes enhanced mixing and thus weakens the upper halocline and stratification. The ultimate result is the shoaling of the Atlantic water (AW) layer, which stores heat that could reduce sea ice formation even further. A conceptual model has recently been proposed that refers to this change as “atlantification” (Figure 5.1, Polyakov et al., 2017).

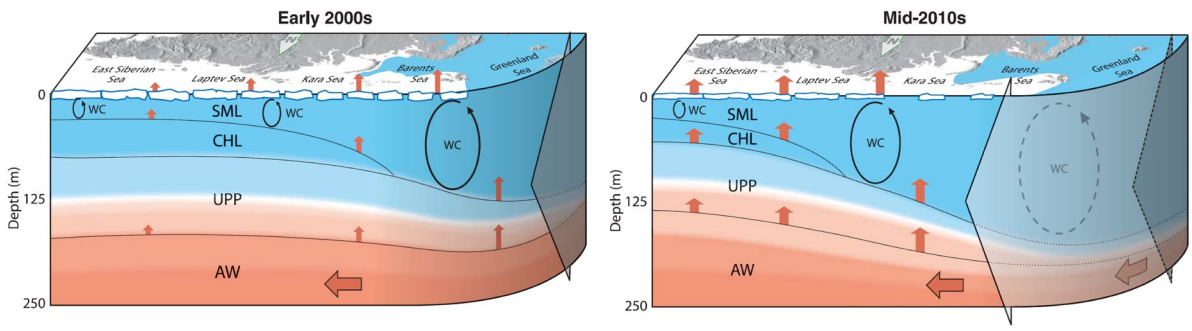

Fig.5.1: Conceptual model of the “atlantification” of the Eurasian Basin (from Polyakov et al., 2017).

Based on past hydrographic surveys, the AW is capped by a fresh and cold surface layer separated by a sharp pycnocline in which salinity increases from <33 in the upper ~100 m to around 34.5 at 150–300-m depth (e.g., Rudels et al., 2015). Frontal structures and the accompanying interleaving and intruding features are universal in the central Arctic Ocean (Rudels et al., 2013). This reflects that the coexisting water masses exchange their properties with each other. The vertical stratification with a relatively warm and saline water mass in the intermediate depths results in double-diffusive staircases, which are believed to be important to transfer the AW heat toward the upper halocline (Polyakov et al., 2012). We will show later that this feature is ubiquitous during Leg 1.

Although various efforts to monitor the ongoing changes in the Eurasian Basin have been made in the past years/decades, direct observations by means of extensive hydrographic surveys especially during winter are still limited. The remoteness and presence of heavier sea-ice conditions in the Amundsen Basin also contribute to the fact that long-term oceanographic observations are less there than those in the Nansen Basin and the surrounding continental shelves. The core temperature of the AW layer in the Amundsen Basin is ~2–3°C lower than that in the Nansen Basin, suggesting a heat loss as the AW spreads and distributes to the ambient waters.

The Arctic Ocean circulation is historically argued being controlled by a thermohaline gradient or wind-driven circulation. Proshutinsky & Johnson (1997) used a two-dimensional barotropic model to show that there are two regimes of wind-forced circulations. The wind-forced circulations alternate between cyclonic and anticyclone circulations, with each regime persisting for 5–7 years. Their model results give convincing patterns of wind-driven circulations, however, only climatological data sets were used to support the modeling results. In-situ measurements of temperatures and salinities from Ice Tethered Profilers (ITPs) indicate a change the wind-driven circulation (M.-L. Timmermans et al., 2011). Note that this conclusion is also derived from a numerical model. A demand of in-situ measurements is thus necessary to evaluate the wind-driven circulation.

Besides double diffusive staircases, dissipation of internal waves provide another means to transfer the AW heat upward and carry fresh water downward. The thinning of the Arctic sea ice coupled with atmospheric forcing raise the potential of near-surface mixing and generation of internal waves. The generation of internal waves in the Arctic Ocean is believed to result from winds and sea-ice motions (D'Asaro & Morehead, 1991). The internal wave energy in the Arctic Ocean is also one to two orders of magnitudes lower than that in the open ocean. This is because the sea ice effectively damps the wind-generated energy for internal wave generation (e.g., Morison et al., 1985). Attempts had been done to determine whether the background mixing increases in response to the diminishment of the Arctic sea ice (Guthrie et al., 2013), however, there is still a clear bias that the measurements were mostly after February. It is still not clear how internal waves evolve, and how related dissipation and turbulence behave in winter.

Due to the existence of surface fresh water, the Arctic Ocean is a region full of filaments and frontal structures. These features are related to frontal instabilities and restratification. In response to these processes, (sub)mesoscale eddies are generated through the release of potential energy. Submesoscale eddies are within a limit of the Rossby radius of O(10 km) and have the ability to carry heat laterally and even trap sea ice out of the ice edge (Manucharyan & Thompson, 2017). Their small scales hinder a proper modeling in general circulation models and their roles among the sea ice-ocean interaction in the multiyear ice-covered central Arctic Ocean still need further investigations.

Clearly, a year-round data set covering different seasons is crucial to determine the current state of the Arctic Ocean in order to obtain a more clear picture to answer the above-mentioned questions and challenges. The year-round data set also provides a means to evaluate the impact of the global rise of the greenhouse gases to the Arctic Ocean. The MOSAiC expedition aims to monitor an ice floe during the year-round drift through the Transpolar Drift, providing us an unprecedented platform to study interactions between the atmosphere, sea ice, and ocean. These efforts are complemented by a distributed network of autonomous platforms, which allows us to study horizontal gradients of thermohaline and flow fields. We expect that the data collected in MOSAiC will provide climate researchers a more comprehensive data set to study the climate, fate, and dynamics of the Arctic Ocean.

2. Arctic Ocean mixing processes and vertical fluxes of energy and matter

The Arctic Ocean is a strongly stratified low-energy environment, where tides are weak and the upper ocean is protected by a sea-ice cover during much of the year. Interior mixing processes are dominated by double diffusion. The upper Arctic Ocean features a cold surface mixed layer, which, separated by a sharp halocline, protects the sea ice from the warmer underlying Atlantic- and Pacific-derived water masses. These water masses carry nutrients that are important for the Arctic ecosystem. Hence vertical fluxes of heat, salt, and nutrients are crucial components in understanding the Arctic ecosystem. Yet, direct flux measurements are difficult to obtain and hence sparse.

During the MOSAiC expedition, we plan to obtain a time series of under-ice turbulence microstructure measurements on the central ice floe in order to determine dissipation rates of turbulent kinetic energy and fluxes of heat (and nutrients). We will operate an MSS90L profiler (MSS), equipped with two shear sensors, as well as fast response temperature, conductivity, acceleration, and turbidity sensors, in free-fall mode at a rate of 1,024 Hz. Due to the patchiness of turbulence in the ocean, a statistically meaningful sampling strategy requires a greater number of casts to average them into one profile. Mixing rates are further strongly dependent on shear that may be forced by sea ice motion, wind-driven currents or tides, which is why the goal is to resolve several full semidiurnal tidal cycles.

One particular project focused on turbulence in the upper Arctic Ocean is AROMA. Funded by the Research Council of Norway, AROMA aims to collect high quality ocean microstructure measurements (manual profiling and autonomous systems), as well as background measurements of currents and stratification during MOSAiC, with the overall goal to advance our understanding of the vertical mixing processes, their role for the heat and nutrients in the Arctic Ocean and the associated feedbacks.

In order to address its objectives, AROMA supplies 3 on-ice installations (autonomous, continuous recording systems, planned to be operative in all legs) and one vertical microstructure profiler to be operated in coordination with the profiling from Ocean City (in all legs). Dissipation measurements in the upper 80 m up to the ice-water interface using an uprising vertical microstructure profiler will be crucial to resolve the under-ice boundary layer and to better quantify the ocean heat fluxes in the upper water column. The background currents in the upper 500 m will be measured using a RDI Workhorse 75kHz acoustic Doppler current profiler (ADCP). These current measurements will supplement ship-board 150kHz ADCP, and will also be closer to the profiling location from the Ocean City. Background current measurements are paramount to describe the forcing conditions and weather-scale (eddies) as well higher frequency (internal wave) variability. The internal wave field, and the background temperature structure in the upper 200 m, will further be sampled using a thermistor string (RBR). The thermistor string is supplemented with 4 (internal logging) CTD loggers. On the same thermistor string, a Rockland Scientific MicroRider is attached (in a separate line) and will collect temperature microstructure data at 60 m depth, continuously. The instrument is enhanced to allow on-board data processing as well. The continuous microstructure time series will supplement the profiling measurements, and will allow quantification of dissipation rate of temperature variance, and estimation of turbulent heat fluxes in different forcing conditions. The final system includes 3 clusters in frames installed at 25, 45, 70 m depth, with each cluster sampling temperature, salinity, pressure, pCO_2, and high-resolution velocity profiles (10 m vertical range) with particular emphasis on resolving the vertical velocity fluctuations. Using the 3-level pCO_2 measurements (3-hourly intervals), we aim to resolve the vertical gradient of pCO_2 in the upper ocean. Combined with eddy diffusivity measurements, we will obtain vertical fluxes of pCO_2. All installations are sufficiently close to each other to be interpreted as a system delivering data from forcing conditions to small scale mixing.

3. Water sampling for CFC/SF6, Helium & Tritium

Processes at the sea-ice edge are especially efficient to enhance the contact between the mixed layer and the halocline by wind-induced upwelling. Processes in leads also enhance strong sea-ice formation, which will trigger both brine-induced and momentum-induced vertical convection. This will inevitably deepen the mixed layer. Leads might be the place of pronounced horizontal gradients, that could restratify the upper ocean by submesoscale processes. To estimate the role of the different processes (upwelling, entrainment, gas exchange, melt and formation of sea ice, energy input through the wind field) we will measure the noble gases ^{3}He, ^{4}He, and Ne as well as CFCs and SF6 in the mixed layer, the halocline, and in the Atlantic Water, and combine them with the concurrent turbulence, current, stratification and meteorological measurements carried out during MOSAiC. The different isotopes and gases are necessary to separate the various processes as they act differently on isotopic rations and concentrations. Buoys observing the near-surface layers within the Distributed Network in a range of 5–25 km from the central observatory will deliver hourly high-resolution (1-5 m) profiles of temperature and salinity between the surface and 100 m depth throughout the drift. This will allow to identify the 3-dimensional structure of the mixed layer and upper halocline year-round. These will be augmented by the essential ongoing measurements of the upper water column by the ship-based CTD/rosette and autonomous profilers up to 15 km away from the ship.

4. General preparations for sustained measurements of ocean properties during MOSAiC

In order to determine water mass properties and their seasonal evolution throughout the entire MOSAiC campaign as described above, the operation of the ship's CTD/Rosette system is of crucial importance. It is the only means to obtain full-depth CTD/net profiles, and it also significantly facilitates the sampling of water to measure a large suite of important variables throughout all involved disciplines. However, the operation of this system is a significant challenge in the extremely low temperatures of the Arctic autumn and winter, mainly due to two reasons: First, frozen sensors due to remaining waters inside may change the sensor reading or damage the sensors permanently when the sensors are exposed to low temperatures for too long. Second, the sampling bottles may also get frozen thus hampering the sampling process itself. These two challenges can lead to the loss of the ability to accurately sample for certain substances. In order to mitigate this effect, a suite of measures needed to be taken, and a procedure to safely operate the CTD/Rosette system in extremely low temperatures has to be developed in order to protect the sensors and to maintain the ability to sample water as planned.

Especially in case the main hydrohole that is necessary to utilize the ship's CTD/Rosette system cannot be created or maintained, a second hydrohole within a sheltered tent on the main ice floe is of crucial importance. This installation is a prerequisite to deploy a smaller CTD/Rosette system, and especially also to operate various other devices, most notably a suite of microstructure probes in order to determine small scale turbulence in the upper water column. However, especially in the autumn and winter months, Arctic sea ice is a highly dynamic and variable regime. The establishment of a stable and sustainable ice camp that would last throughout the entire duration of the MOSAiC drift is considered as one of the biggest challenges of the entire project. Therefore, in addition to establish and maintain a large enough hydrohole through which the ship's CTD/Rosette and the different net systems can safely be operated, a Weatherhaven shelter needs to be installed in a stable location in a safe distance to the ship. This structure is hereafter referred to as Ocean City. Furthermore, the Leg 1 team aimed to identify the safest, most efficient, and sustainable operations with respect to oceanic measurements in order to lay the foundation for the work of all future Legs.

5. Digital Thermistor Chain (DTC) Network

Thermistor chains with the ability to record air, snow, ice, and ocean temperatures are widely used on autonomous ice mass balance buoys (IMBs), which record the evolution of sea ice thickness and snow depth at a fixed site. Recent developments also enable those thermistor chains to also record the temperature rise after a period of active heating. Using this technology, important changes in the seasonal evolution of an ice cover can be detected, such as surface flooding, snow ice formation, melt onset, melt pond formation & -refreezing, as well as internal melt & -refreezing.

In currently available IMBs, these thermistors chains are usually closely tied to a specific electronic setup, making it impossible to operate them independently. However, recent developments enable them to be operated on any platform equipped with an RS232 interface. In combination with other improvements, such as increased resolution, sturdiness, and reliability, it is now the right time to look for applications beyond their use in (expensive) IMBs.

During the MOSAiC drift, the prototype of a distributed network of such thermistor chains shall be deployed on the ice floe where *Polarstern* is anchored. Powered by regular lead batteries and controlled by an affordable, commercially available microcontroller, the units will send their temperature and heating profiles in fixed intervals (e.g. 1 h) or on request to a central receiving unit on the ship via a direct communication link. Based on the incoming data in combination with high-resolution electromagnetic thickness surveys, a 3D temperature and thermal property map of the ice floe and the surrounding atmosphere and ocean is generated, which is then used to calculate sea ice thickness and snow depth in the covered area. Complementing regular sea ice thickness and snow depth surveys by other methods, this information is expected to be very valuable for many studies during MOSAiC.

6. Auxiliary work & installations

In addition to the planned work described above, it was the responsibility of Team Ocean to deploy various sensors and installations for a number of associated projects in order to augment the observational capacity related to sea ice and oceanography. Due to their variety, we do not provide a scientific background here. To summarize, we deployed a biogeochemical sensor suite at a FYI location at the dark site; we installed an acoustic recorder at a SYI location at the dark site; we deployed a SIMBA-type thermistor chain ice mass balance buoy and a snow buoy at a SYI location at the dark site; we deployed 2 UpTempo buoys within the Distributed Network; we deployed 2 T-POP delayed ocean profilers and installed one more thermistor chain ice mass balance buoy close to Ocean City 1.0. Finally, we contributed different CTD sensors for operation on the Remotely Operated Vehicle (ROV). Deployment of the VMP Upriser turbulence probe was not done due to a lack of space, time and personnel.

A detailed report of the installation of a large number of buoys of different types within the Distributed Network onboard the *Akademik Fedorov* is given in a separate document.

Work at sea

Preparation of a large hydrohole close to the ship

One of the main challenges of MOSAiC with respect to measurements of ocean properties was the possibility to regularly operate the main CTD/Rosette system through a hydrohole in the ice close to the ship. This ability was also of particular importance with regard to the extensive water sampling program planned for MOSAiC by Teams OCEAN, ECO and BGC, and further enforced by their high demand of sample volume. The Ocean City CTD/Rosette system is simply not large enough to accommodate such high water volumes, and the small size of the weatherhaven tent couldn't accommodate more than 3 scientists for water sampling at once. Although a plan for creating a large hydrohole close to the ship was established early on, we had to postpone the actual work a few times due to the dynamic nature of the ice close to the ship. The relative movement of the ship and the ice floe itself was still significant,

especially during several storm systems in October and November. One consequence of these storms were that the ice right at the ship's hull became significantly deformed, reaching thicknesses well over 4 m. There was no way of creating a hydrohole as large as 3 x 3 m through such thick ice, with the additional danger of the hole being destroyed by additional ice pressure, or big blocks of ice rafting under the hole. These conditions ruled out the regular CTD operation right next to the ship, and a new plan had to be prepared. We finally came up with the idea to operate the main CTD winch through a block attached to the large crane that is usually used to lift cargo. Benefitting from the extended reach of the crane, we were able to move the location of the CTD hole approximately 8-10 m away from the ship, where the ice was only about 2 m thick.

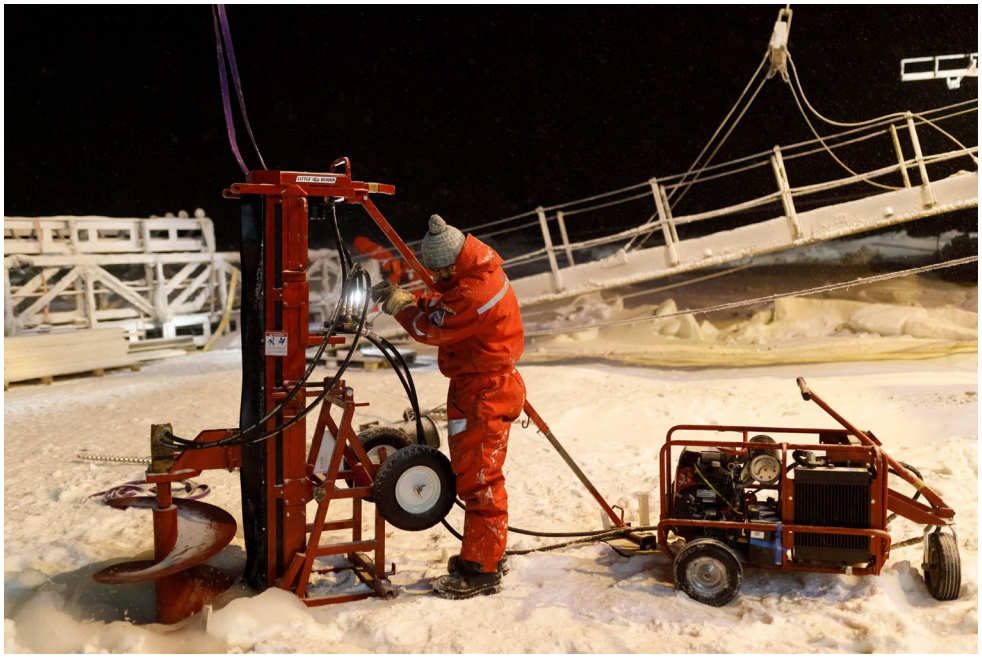

Fig.5.2: Operation of the "Little Beaver" hydraulic drill close to the ship.

During an extended period of relatively stable weather and ice condition early November 2019, the work on drilling the ice hole was started. We took this opportunity to test the newly acquired Little Beaver hydraulic tower drill system, hereafter referred to as "Beaver" (Figure 5.2). The Beaver was lifted on the ice using the crane, and the tower was fixed on the ice with ice screws. It turned out that the system was very challenging to operate. The weight of the Beaver was too heavy to be manually moved, and the friction of the drill was so high that the ice screws could barely hold the tower with the drill. Even after we stabilized the tower using several auger flights, it could still not be operated safely. An additional challenge (besides the low temperatures dropped to -30°C) was also to install and remove the extension necessary to drill through the 2 m thick ice. It took 2 experienced people about 2-3 hours to drill one hole of 60 cm diameter. After a re-assessment of our strategy, we abandoned the Beaver and used two 10-inch auger systems, one of which had an extension installed. Using the swiss-cheese technique, we drilled a number of slightly overlapping holes along square outlines with side lengths of around 1.2 m. We drilled holes through the middle of four ice blocks, and fed a wooden stick through them that was attached to a rope. In this way, they could easily be lifted out with the ship's crane. This work took 3 people around 4 hours. This resulted in a hydrohole of around 2.8 x 2.8 m, which could easily accommodate the CTD/Rosette system (see Figure 5.3). The edges of the hole were secured with wooden plates for safe operations. A rope around the entire hydrohole was fixed on the ice with ice screws as an attachment point for safety harnesses. This was necessary to mitigate the risk of falling into the hole during CTD

operations, or when cleaning ice in the hole. A submersible pump was used to mitigate ice growth in the hole. A lid was constructed to cover the hydrohole when no CTD/net operations took place.

Fig.5.3: View from the working deck of the main hydrohole for operation of the main CTD/Rosette and the different nets. Every other day, the hydrohole had to be cleared of newly-grown ice before CTD operation. When no instruments were operated in the hole, it was covered by a wooden lid for isolation and safety reasons (the wooden lid is in the lower central part of the figure).

Operation of the main CTD/Rosette system in very low temperatures

Due to the susceptibility of the CTD/Rosette system to low temperatures, a procedure was developed to protect the sensors and prevent the samples from freezing while the CTD/Rosette is transported from the hydrohole to the sampling room (Figures 5.4 and 5.5). This procedure is summarized here:

Plastic curtains were installed in front of the sampling room in order to minimize the time of the CTD/Rosette system was exposed to the cold. This area was permanently heated by two 15 kW heaters. A custom made metal cage with a thick plastic sheet was prepared to cover the CTD/Rosette system while transported between the hydohole and the sampling room. This construction is referred to as the “shelter”, which was additionally equipped with isolation material, heating blankets, and two inlets for warm air supplied via tubes by a powerful heating system based on the working deck. The entire procedure is described in great detail in a separate document. There was no single case in which the sensors froze, although temperatures were as low as -30 °C. Occasionally, the water outlets of the Niskins froze, which could however be mitigated by pointing an additional heater towards the system during transport to the sampling room

*Fig.5.4: Deployment of the CTD/Rosette in very low temperatures; **A** Position of pallet and shelter in front of the CTD room. **B** Conus-shaped adapter piece that is mounted on the CTD wire in ordert o fix the shelter. **C** Shelter with CTD/Rosette. **D** Simultaneous operation of crane and winch in order to deploy the CTD in the hydrohole several meters from the ship. **E** Stabilization of the shelter using hooks. **F** Positioning of the CTD/shelter combo on the hydrohole. **G** Removal of the winch wire from*

the shelter while the CTD is parked at 10 m depth. ***H*** *Position of shelter next to the hydrohole while the CTD is profiling.*

Fig.5.5: Retrieval of the CTD/Rosette in low temperatures; ***A*** *Installation of venting system to provide warm air into the shelter.* ***B*** *Positioning of heater within the shelter while parked next tot he hydrohole.* ***C*** *Pulling the shelter over the hydrohole.* ***D*** *Guiding the winch wire into the shelter.* ***E*** *Heaving of the*

CTD/Rosette into the shelter. ***F*** *Heaving of the CTD/shelter combo onto the deck.* ***G*** *Heating the CTD/Rosette during removal of the shelter on the working deck.* ***H*** *Continuous application of warm air during transport of the CTD/Rosette into the sampling room.*

Summary of the ship-based CTD/Rosette work

The *Polarstern* CTD/Rosette has a 24-position layout with 24 12-liter OTE bottles. A standard SeaBird 911 plus system was vertically attached to the rosette equipped with double sensors for temperature, conductivity, and oxygen, and sensors for pressure, fluorescence for Chl.*a* and CDOM, irradiance, beam transmission and nitrate (Table 5.1). The system was additionally equipped with an Underwater Vision Profiler (UVP, see Team ECO chapter 6.2). Finally, an altimeter was mounted to monitor the distance to the seafloor (and which started to catch an echo at ~40 m above the bottom). Deep CTD casts were done to ~10 m above the seafloor. The actual water depth matched the calculated and sound-speed corrected EK60 water depth with an uncertainty of 2 m.

Ship-based CTD casts were done regularly up to four times a week, and usually on Thursday and Friday (and occasionally on Saturday). The water budget and sampling sequences of different parameters was discussed among the different teams before each cast. During Leg 1, Team BGC only requested a minor amount of water samples from the ship-based CTD/Rosette, while the majority of the water demand came from Team ECO. Team OCEAN required water samples for CFC/SF6 and salinity calibrations during deep (>1000 m) casts, as well as water samples for CFC/SF6, helium and tritium from shallow casts (< 500 m). Based on the discussion, Team ECO prepared a draft water budget plan for the ship-based water samplings. It was Team OCEAN's responsibility to prepare and operate the CTD/Rosette system, while TEAM ECO's contribution was to keep the CTD hole clear of ice.

A shallow CTD cast was usually conducted first, followed by various net deployments. A deep cast was performed in the afternoon. A full depth cast to 4400 m took about 4 hours. Overall, 19 CTDs were deployed from *Polarstern*, four of which were deep casts (see Table 5.7). Once the water sampling was finished, the raw CTD data was pre-processed following the Seabird procedures. The data was provided to the MCS, and quicklooks were made available (see Preliminary Results section).

Tab.5.1: Sensor configuration of the *Polarstern* CTD/Rosette system. Sn = serial number.

	Temperature sensor	**Conductivity sensor**	**Oxygen sensor**	**Pressure sensor**	
Primary	SBE3 sn #1338	SBE4 sn #3173	SBE43 sn #1834	sn #0321	
Secondary	SBE3 sn #1374	SBE4 sn #3590	SBE43 sn #0467	-	-
Altimeter	**Transmissometer**	**Nitrate sensor**	**Chl-a Fluorometer**	**PAR/Irradiance sensor**	**CDOM Fluorometer**
Sn 47768	WET Labs C-Star sn #1198	Satlantics SUNA sn #0732	WET Labs ECO-AFL/FL sn #725	Biospherical/ Licor sn #70257	WET Labs ECO CDOM sn #4531

Ocean current measurements by shipboard ADCP

Polarstern is equipped with a shipboard ADCP (S-ADCP) to monitor underway ocean currents. The installed ADCP model is a RDI 150 kHz Ocean Surveyor system. Due to potential interferences between the S-ADCP and the various fish sounders used during MOSAiC, a K-

sync system was used to alternately triggered the different instruments. By using this system, we expected to avoid potential conflicts and interferences between the acoustic devices, which however came with the compromise of reduced data quality especially of the current measurements. Upon the arrival of the Leg 1b Team OCEAN on 17 October, the S-ADCP and fish sounder data quality was re-examined together with the ship IT and Team DATA specialists. It was concluded that there was no apparent interference between the S-ADCP and the fish sounders even when they were operated simultaneously. Moreover, the acoustically backscattered energy level was much lower than for example in mid-latitude oceans. A significant acoustic energy loss was found below ~250 m. We thus modified the ADCP configuration file on 28 October, changing the bin size from 4 m to 8 m to have a higher backscattered energy level. After a preliminary processing of the raw S-ADCP data, we concluded that the vertical coverage of underway currents was within ~20–240 m, using a long-term averaged interval of 20 min and a short-term averaged interval of 5 min. We conclude that all data obtained before the change on 28 October is questionable in terms of quality and recommend to treat this data cautiously

Installation of Ocean City 1.0

Preparation and initial installation of Ocean City was mainly done by the Leg 1 a Team, with the support of many helpers from other teams. A hydrohole of 1.3 x 1.3 m was prepared in an area of level ice of around 0.6 m. An array of floatable plastic pontoons was assembled above the hydrohole (Figure 5.6), and a wooden floor was built on top of them. Two big and heavy winch systems were planned to be used in Ocean City: an AWI custom-built system for the CTD/Rosette, and a KC Denmark winch for net operations. Due to their size and weight, they were placed on the platform before the actual tent was installed. The CTD/Rosette frame was also placed on the wooden floor, after which the Weatherhaven tent was finally mounted around them. The tent was fixed to the ice with 6 straps using ice screws. The sides were covered by snow for insulation. The Ocean City power hub was installed at a distance of 10 m. Two separate power cables were installed between the hub and the tent, where they were connected to two fuse boxes. A lid to cover the CTD hydrohole was constructed, but was later replaced by a more convenient “bridge”. Two 3 kW heaters running on thermostats were operated to keep the temperature above +5°C in order to protect the sensors from freezing. A submersible propeller pump was used to keep the hole ice free. The hole anyways needed to be cleared of ice forming at the edges every other day using a chisel and ice saw. Further equipment, including the winch control boxes and CTD deck unit were arranged on tables. The custom CTD winch broke down after an initial test due to being used in too low temperatures. A temperature relais needed to be uninstalled to resume its operation.

Fig.5.6: Initial setup of Ocean City (photo: Julia Regnery)

The exchange of Team OCEAN personnel between Leg 1a and 1b took place on 17 October. It turned out there was a big piece of rafted ice at 2 m depth below the hydrohole. This ice could almost be cleared, but some remains to the side of the hydrohole hampered MSS operations throughout the lifetime of Ocean City 1.0. Further configuration and final installation of instruments and sensors inside Ocean City took until 22 October. After the modification of the CTD winch, it worked generally well. However, the tent was slightly tilted, and the automatic cable guidance system couldn't work properly. As a result, the cable was damaged at some point and it needed to be re-terminated. The KC Denmark winch, which was planned for the operation of nets in Ocean City, was never used during Leg 1.

The first official MSS and CTD deployments in Ocean City were commenced on 22 and 24 October, respectively.

A strong wind event with peak wind speeds of ~20 m s^{-1} struck the main ice floe between 16–18 November, causing many cracks, leads, and newly-formed ridges, also with concurrent power outages. A large fracture zone led to a separation of the main ice floe into two pieces. The nearby Remote Sensing City and Met City drifted away from Ocean City and Balloon Town on 17 November. A ~30-m wide lead was formed ~15 m away from Ocean City. This lead eventually transformed into a growing ridge, which kept approaching Ocean City. On 20 November, the ridge had grown to ~5-m height, and was only a few meters away from Ocean City. As a side effect, a big piece of rafted ice appeared below the Ocean City hydrohole. After we tried to push it back under the ice away from the hole, it eventually rose up and blocked the hole entirely. We decided at this point to maintain the hole, and tried to remove the ice block by cutting it into several small pieces. After two more hours, several cracks appeared in the surrounding area, with one widening crack even passing through the Ocean City hydrohole. This was the moment when the decision was taken to disassemble Ocean City and move it to a new location.

Fig.5.7: Relocation of Ocean City 1.0 (blue tent) on 20 November 2019 using an ARGO vehicle (photo: Johannes Käßbohrer). The decision was made due to a combination of several factors: a) a number of cracks appeared in the closer surroundings; b) a significant ridge along the main floe's shear zone was approaching the site (distance at time of evacuation: ~15 m); c) the hydrohole was blocked by a rafted piece of ice; and d) a crack was opening up through the hydrohole.

However, due to the size and weight of the gear inside the Weatherhaven, disassembly was not straightforward. First, we evacuated the power hub and the sensitive equipment from the tent. We then decided to try to move the entire tent, including the pontoons, with the Argo vehicle, rather than unmounting the entire tent. Several big straps were spanned around the pontoons to maximize the stability of the construction, and a Kevlar rope was used to attach the tent to the Argo. It took several attempts to get it moving, also because the pontoons were partly frozen to the ice surface. Due to the weight of the tent and its contents (probably almost 1.5 tons in total), the Argo was almost at its maximum pulling capacity. Due to the unclear ice and storm situation, we decided to drag the tent towards safe ground in the logistics area (Figure 5.7). Unfortunately, we had to cross the BGC coring area because of the limited maneuverability. The evacuation went comparably smoothly, without any loss of equipment or damage of sensors and installations.

Installation of Ocean City 2.0

After the storm had passed, surveys for a new site were started. A suitable location was identified on 21 November 2019, about 50 m away from the fracture zone and 50 m from the old location. A new hydrohole was prepared by chain saw on 22 November. The tent was dragged back on the same track through the BGC coring area. We decided to let the surroundings refreeze before placing the Weatherhaven atop it in order to avoid the freezing of the pontoons to the ice. We placed the tent atop the new hydrohole on 23 November using the Argo, and fine-tuned the alignment on the hole manually with 6 people. Further assembly and final preparations of sensors were done one day later. Ocean City 2.0 was born and fully operational on 25 November (see Figures. 5.8 and 5.10). Expecting that such a breakup could happen any time again, the towing straps were left in place. This practice provided us a valuable experience how to deal with evacuation of significant infrastructure, and showed the importance to have constructions that are flexible and support short-term relocations.

Fig.5.8: The relocated Ocean City 2.0.

CTD/Rosette casts in Ocean City

The CTD/Rosette system in Ocean City is essentially a smaller version of the ship-based CTD/Rosette. The rosette has a 12-position layout with 12 5-liter OTE bottles. In the lower part of the frame, a standard SeaBird 911plus system is mounted, equipped with double sensors for temperature, conductivity and oxygen, as well as sensors for pressure, Chl-a fluorescence, irradiance, beam transmission, nitrate, and methane concentration/gas temperature (see Table 5.2). The custom-built winch can support safe ascending/descending speeds of ~0.2–0.5 m s^{-1}, and has a cable length of 1500 m. A typical 1000-m profile normally takes about ~3 hours. Overall, 30 CTD deployments were done in Ocean City. Among these deployments, water samples were taken primarily for Team BGC, which are interested in shallow depths (~120 m). Water samples were also collected occasionally for salinity calibration and CFC/Helium/Tritium samples. Similar to the ship-based CTD/Rosette data, post-processed data were copied to the MCS, and quicklooks were prepared (see Preliminary Results).

Tab.5.2: Sensor configuration of the Ocean City CTD.

	Temperature sensor	**Conductivity sensor**	**Oxygen sensor**	**Pressure sensor**	
Primary	SBE3 sn #4918	SBE4 sn #3549	SBE43 sn #1605	sn #0935	
Secondary	SBE3 sn #5110	SBE4 sn #3810	SBE43 sn #0743	-	-
Altimeter	**Transmissometer**	**Nitrate sensor**	**Chl-a Fluorometer**	**PAR/Irradiance sensor**	**Methane sensor**
N/A	WET Labs C-Star sn #1220	Satlantics SUNA sn #1318	WET Labs ECO-AFL/FL sn #1346	Biospherical/Licor sn #70241	Franatech METS sn #1917

Turbulence measurements in the upper water column

An MSS turbulence profiler (MSS90L, SEA & SUN Technology, Germany) was regularly deployed from Ocean City to a depth of 400 m. A profile took around 20 min. If time allowed, those profiles were combined with a 400-m CTD cast that also included the Satantics SUNA

nitrate sensor in order to later be able to calculate nitrate fluxes. Due to the statistical data processing approach that is necessary to obtain vertical fluxes, we tried to always take at least 4 consecutive MSS profiles during a session. In total, 168 MSS profiles were recorded during Leg 1 (see Figure 5.9 and Table 5.8).

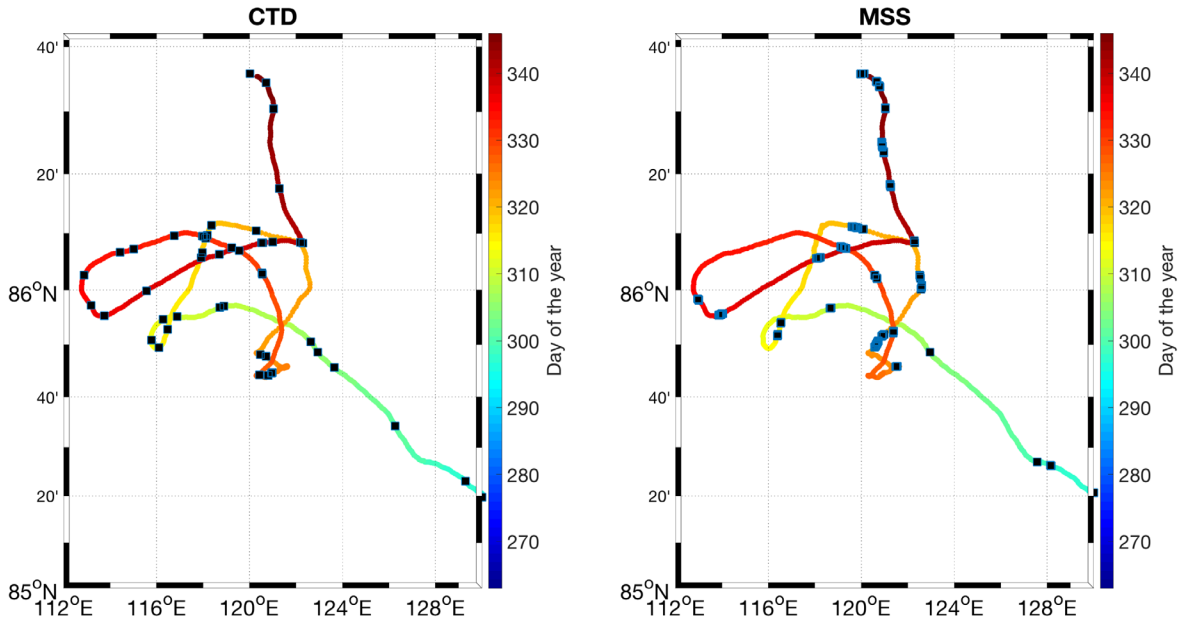

Fig.5.9: CTD (left) and MSS (right) measurements (squares) commenced after Ocean City is operational. The ship track is color coded by day of the year.

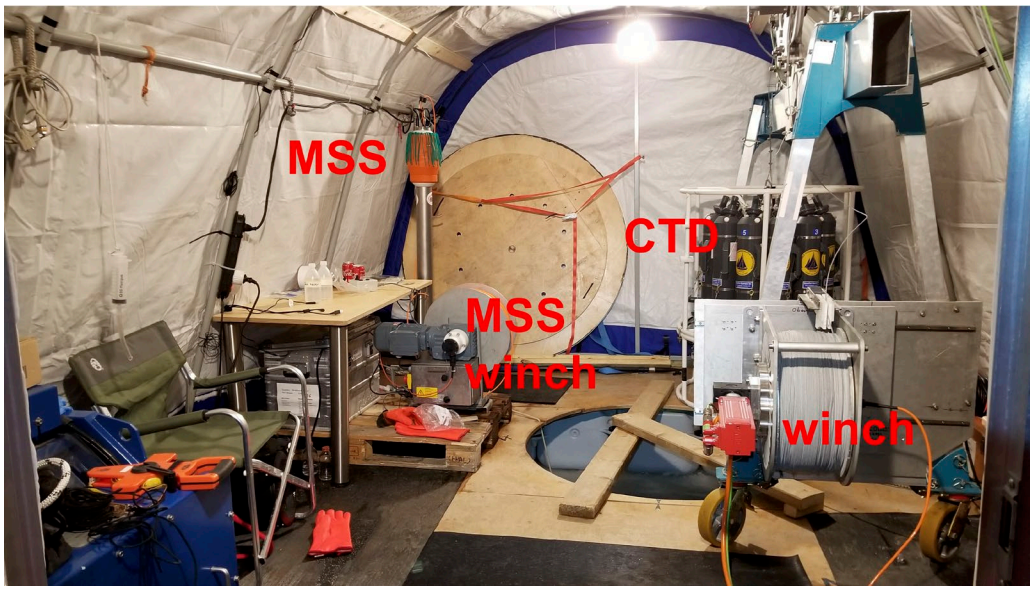

Fig.5.10: Interior view of the Ocean City 2.0 weatherhaven tent. The hydrohole is below the circle-shaped hole next to the MSS winch, and was usually covered by a small bridge for easy passage.

Fig.5.11: Preparation of LISST on the ice hole (left) and mounting the instrument underneath the CTD/Rosette with four rope shackles (right).

Laser In-situ Scatter Transmission meter (LISST)

In addition to the standard CTD and MSS measurements, a Laser In-situ Scatter Transmission meter (hereafter referred to as LISST) was used in order to measure underwater distribution of particle sizes. Measurements from this instrument were taken within the framework of a project of the Polar Research Institute of China (PRIC) in order to collect time series of particle sizes in the upper 500–1000 m of the ocean throughout the entire MOSAiC drift. The instrument frame was attached to the Ocean City CTD/Rosette using four rope shackles. The frame was mounted perpendicular to the CTD sensor inlets. Regular CTD operation as well as overall data quality of the Ocean City CTD was not affected by the addition of the LISST below the CTD rosette, as long as it was mounted in a perpendicular way. On 23 November we tried to mount the sensor onto the ship-based CTD/Rosette system, but the data quality was significantly reduced. We attribute this to the CTD being vertically mounted, leading to the intakes receiving the wake flow passing the LISST. Further LISST deployments from the *Polarstern* CTD were not done. Whenever time permitted, the LISST was deployed along with the Ocean City CTD twice a week and down to 500–1000 m. Mounting the LISST below the CTD/Rosette was done using two wooden bars placed onto the hydrohole (Figure 5.11, left). The LISST was placed nto the bars and the CTD/Rosette was lowered until the frame could be attached by the rope shackles (Figure 5.11, right). Mounting and unmounting the instrument took about 15 min. Due to the load limit of the CTD winch of about 200 kg, water samples were not taken during a LISST deployment. The dry weight of the CTD rosette is ~130 kg, plus 60 kg for twelve full Niskin bottles. The dry weight of LISST is ~40 kg. A detailed description of LISST operation is available in a separate document. Overall, 10 LISST profiles were obtained during Leg 1, nine of which were obtained from Ocean City and one was based on the ship. Date and related information are given in Tables 5.6 and 5.7. For more detailed information, see Team ECO chapter.

Sampling for CFC/SF6, Helium & Tritium

Most CFC/SF6, helium, and tritium samples were taken during the ship-based CTD operations. Ampoules for sampling CFC/SF6 were prepared one day prior to the planned CTD cast. Metal accessories of the ampoules were examined, rinsed, and cleaned before sampling. The sampling scheme for these samples was twofold, one was for deep-water casts and the other was for shallow-water casts The deep-water samples below 1000 m were usually collected during the regular Thursday CTD operation (after 9 November). Note that only CFC/SF6 were sampled for CTD operations on Thursday. The shallow-water samples were usually performed

on Fridays after a ~500 m cast. For the shallow-water casts, CFC/SF6 and Helium were sampled together, and tritium was sampled every 2–3 weeks. After several water budget meetings on board with Teams ECO and BGC, it was agreed that CFC/SF6 (and helium) have the first priorities for the designated bottles. The naming convention for each sampled ampoule follows the D-Ship station id. For example, the samples taken on 9 November had the D-Ship station id PS122/1_6-81. A sample taken from bottle #1 closed at 3000 m for example had a label called PS122/1_6-81/1/3000. The same rules apply to sampled copper tubes and tritium bottles. Flamed ampoules and sampled copper tubes and tritium bottles were dried and then carefully stored in their original boxes. Information on CFC/Helium/(Tritium) samplings are provided in Tables 5.6 and 5.7.

Fig.5.12: Preparation of CFC sampling (left) and flame-sealed CFC/SF6 ampoules (right).

Sampling for helium and tritium is relatively straightforward. Helium was sampled in copper tubes. Tritium was sampled in plastic bottles. CFC/SF6 is sampled using specific fragile ampoules, and is rather challenging (Figure 5.12). The procedure is summarized in a separate document.

Sampling was also attempted in Ocean City, but turned out to be challenging. Among other factors the constrained space and lower bottle pressure were the biggest problems. Several ampoules broke during transport to *Polarstern*, resulting in a high sample loss ratio. These experiences have been transferred to the Leg 2 team, which will hopefully come up with a better sampling strategy in Ocean City.

Installation of AROMA turbulence moorings

In order to address its objectives, AROMA contributes 3 permanent installations on the main ice floe. These autonomous, continuous recording systems are planned to be operative in all legs. In addition, one vertical microstructure profiler is planned to be operated in coordination with the profiling from the Ocean City during all legs. Dissipation measurements in the upper 80 m up to the ice-water interface using this uprising vertical microstructure profiler will be crucial to resolve the under-ice boundary layer and to better quantify the ocean heat fluxes in the upper water column.

ADCP Longranger mooring

A RDI Workhorse 75kHz acoustic Doppler current profiler (ADCP) was deployed 50 m from Ocean City 2.0 in order to measure the background currents in the upper 500 m (Figure 5.13). These current measurements are intended to supplement ship-board ADCP measurements, and will complement the MSS turbulence measurements taken in Ocean City. Background

current measurements are paramount to describe the forcing conditions and weather-scale (eddies) as well higher frequency (internal wave) variability.

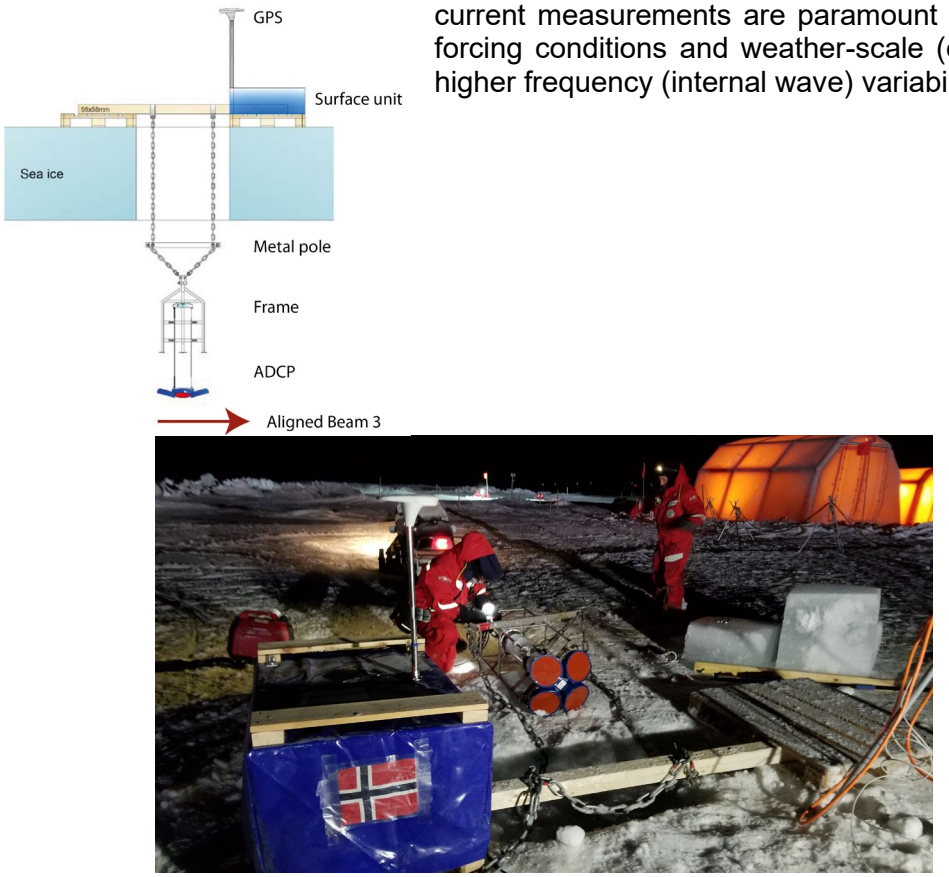

Fig.5.13: Scheme of RDI 75kHz Longranger ADCP mooring (left) and preparation for deployment (right).

Ocean thermistor chain and Microrider mooring

A thermistor string with 24 thermistors at 8 m spacing (RBR, Halifax, Canada) was deployed close to the snowmobile parking lot in the logistics area on 15 December 2019. The purpose of this installation is to record the internal wave field as well as the background temperature structure in the upper 200 m of the ocean. The temperature data is recorded every 30 seconds, and is internally logged via a RBR concerto datalogger attached to the mooring chain at 3 m depth. On the same mooring line, a Rockland Scientific MicroRider is attached on a separate cable, which continuously collects temperature microstructure data at 50 m depth (Figure 5.14a, b). The instrument is enhanced to allow on-board data processing as well. The continuous microstructure time series will supplement the profiling measurements, and will allow quantification of dissipation rate of temperature variance, and estimation of turbulent heat fluxes in different forcing conditions. Data of the RBR thermistor string and the Microrider are also remotely accessible using an Ethernet connection via a RadioLAN link from the main power hub.

The thermistor string is further supplemented with 4 internally logging only RBR CTD recorders, which need to be retrieved at the end of the drift to gain access to the data.

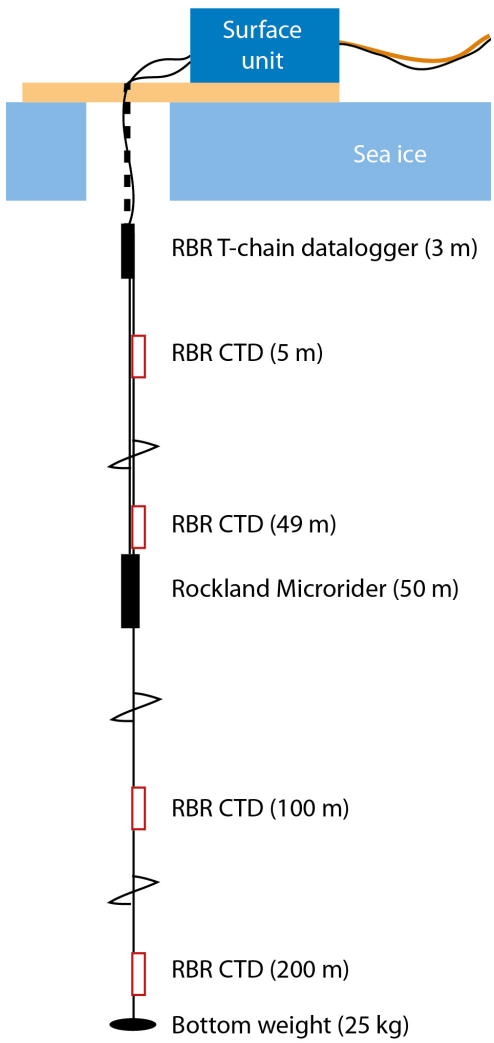

Fig.5.14a: Thermistor chain / Microrider mooring scheme.

Fig.5.14b: Thermistor chain / Microrider deployment

Cluster mooring

The cluster mooring consists of three individual instrument clusters, each holding a SBE37 CTD, a Nortek S1000 ADCP and a SAMI PCO2 instrument as well as a subsurface communication box (Figure 5.15, Table 5.3). The individual frames are installed at 25, 45 and 70 m depth. Three sets of instruments are mounted in a respective metal frame, and the three frames are attached onto each other by Kevlar ropes (see Figure 5.16). The S1000 ADCP is mounted on a foldable arm, looking downward. A weight of 25 kg is attached at the bottom of the mooring. The total weight is around 200 kg in air. All instruments are connected to the corresponding subsurface communication box, each of which contains a serial-to-ethernet converter (Moxa NPort). A single ethernet communication cable goes from each cluster to the surface unit. The surface unit is a pelicase embedded inside a blue buoyancy pallet. The system is connected to a power hub via power and data cables. Through this setup, the individual instruments can be connected to via the *Polarstern* network, and data can be downloaded via the corresponding software on a regular basis.

Due to the general setup and weight of the system, the deployment was very challenging. We attached the Kevlar ropes to snowmobiles rather than using a Tripod for the deployment, in order to simplify and speed up the procedure. Since the SAMI pCO2 sensors are especially sensitive to cold temperatures (>-4°C recommended, air temperature during deployment was -28°C), one cluster was deployed at a time, and the pCO2 sensor was kept warm throughout using an isolating blanket, a generator and a heat gun. The other clusters were stored in Ocean City in the meantime. After one cluster was safely in the water, the next one was carried to the deployment site, and put in the water as quickly as possible.

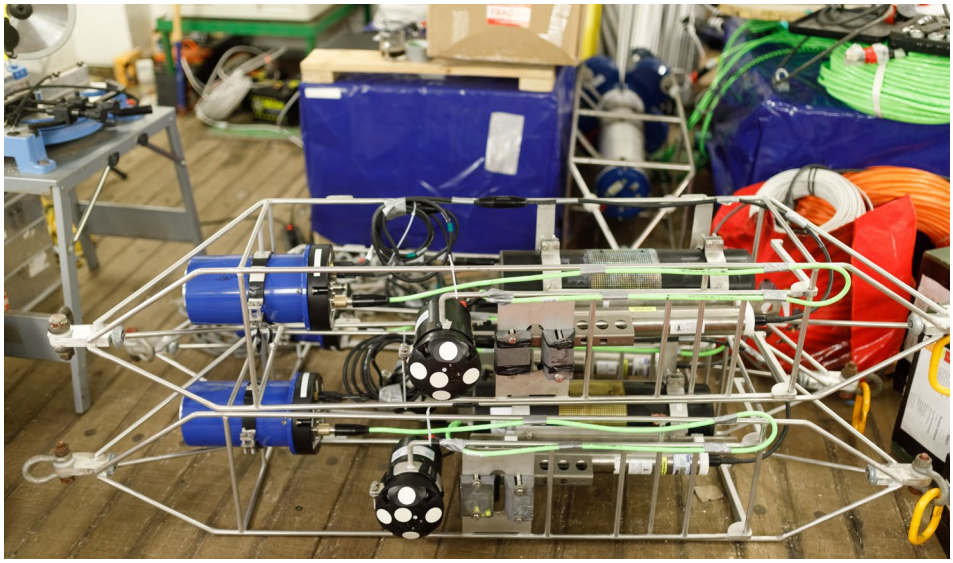

Fig.5.15: Assembled clusters

Each cluster samples temperature, salinity, pressure, pCO2 and high-resolution velocity profiles (10 m vertical range) with particular emphasis on resolving the vertical velocity fluctuations. Using the 3-level pCO2 measurements (3-houry intervals), we aim to resolve the vertical gradient of pCO2 in the upper ocean. Combined with eddy diffusivity measurements, we will obtain vertical fluxes of pCO2. All installations are sufficiently close to each other to be interpreted as a system delivering data from forcing conditions to small scale mixing.

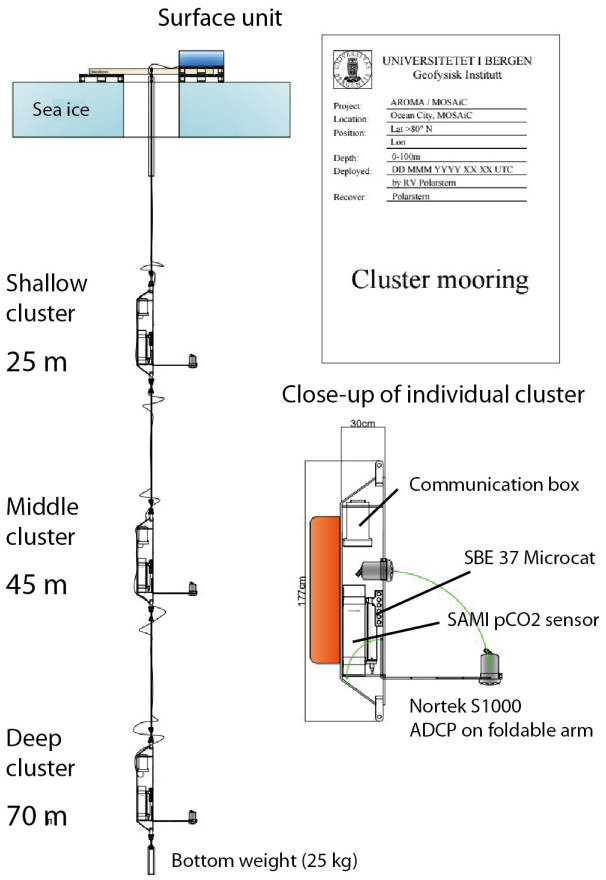

Fig.5.16: Left: Scheme of cluster mooring. Right: deployment of the cluster mooring. Each of the three individual components comprised a metal frame with a Nortek S1000 ADCP on a foldable arm, a Seabird SB37 Microcat, a SAMI pCO2 sensor and a MOXA Nport network controller mounted into a SubSeaTech housing.

Tab.5.3: Configuration of the cluster mooring

Name	Shallow Cluster (top)	Middle Cluster (middle)	Deep Cluster (bottom):
IP address	192.168.3.162	192.168.3.161	192.168.3.165
ADCP	Nortek S1000: SN 105 (IP 192.168.3.197)	Nortek S1000: SN 060 (IP 192.168.3.198)	Nortek S1000: SN 154 (IP 192.168.3.199)
CTD	SBE37 Microcat: SN 8972	SBE37 Microcat: SN 8970	SBE37 Microcat: SN 7224
pCO2	SAMI pCO2: SN C0209	SAMI pCO2: SN C0210	SAMI pCO2: SN C0208

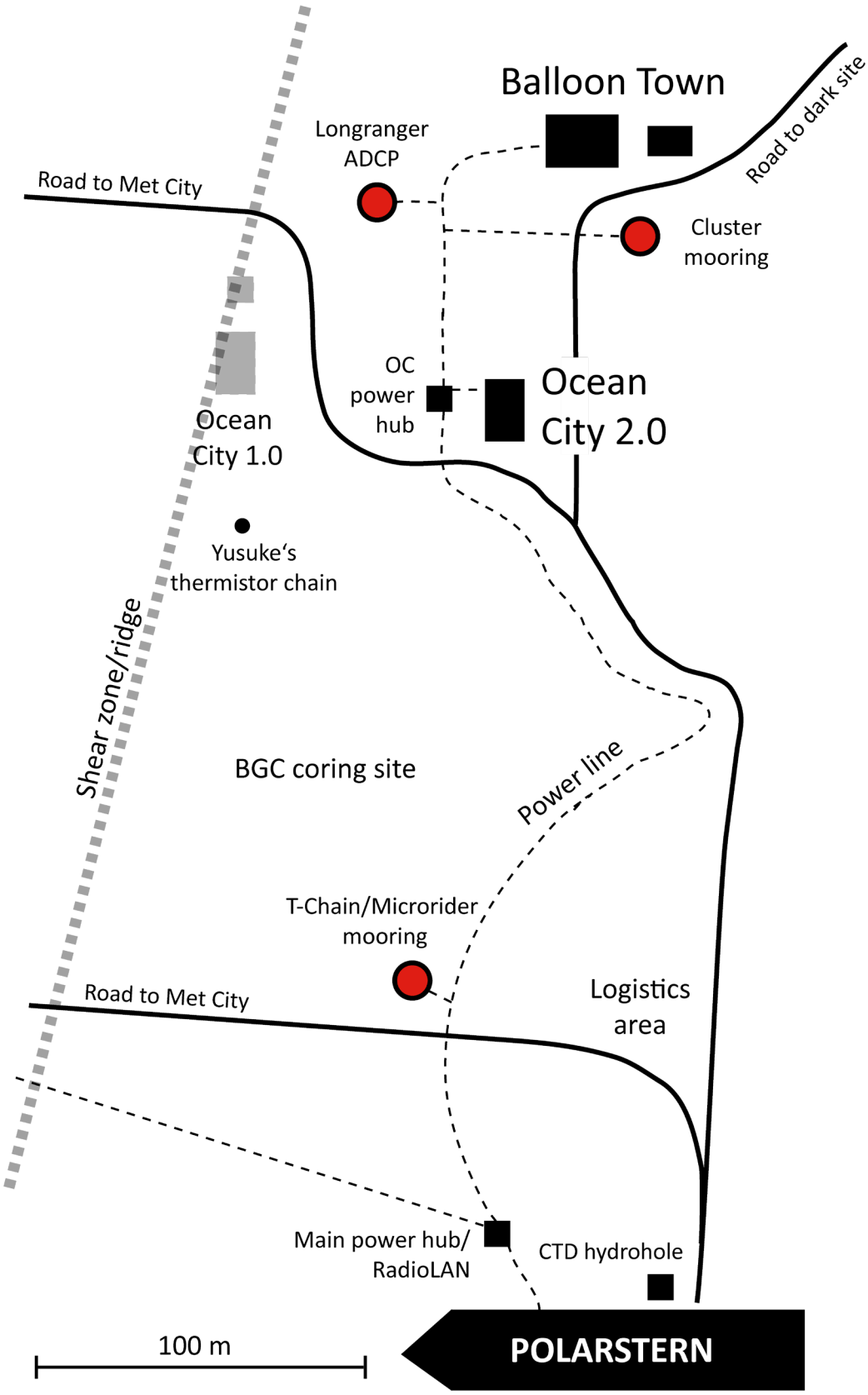

Fig.5.17: Schematic of the Central Observatory around Ocean City, including major power lines, roads, waypoints and important installations.

Installation of other platforms

Thermistor chain buoy (PI: Y. Kawaguchi)

A thermistor chain of the type IceTC2/30 (Marlin-Yug, Russia), consisting of a 2-m long cable with 17 integrated thermistors was deployed close to Ocean City 1.0 on 11 November 2019 (see Figures 5.17, 5.18). Near-real time temperature data of the ice interior and upper water underneath the ice is reported back via Iridium on a regular interval. The deployment is part of the project "Measurement of lee waves and turbulent heat flux behind ice keels in ice-ocean boundary layer" of the University of Tokyo.

Fig.5.18: Deployment of IceTC2/30 buoy

T-POP deployment (PI: C. Heuze)

The T-POP is a football-sized autonomous temperature sensor that sits at the bottom of the ocean for a pre-set time, taking measurements every half hour. It then automatically burns its anchoring link to float back to the surface and send its data by satellite. Two out of a total of ~25 of such sensors were deployed during Leg 1 immediately after two near-bottom CTD profiles on 14 November and 28 November (see Figure 5.19). These sensors are part of the project "*Why is the deep Arctic Ocean Warming? (WAOW)*" of the University of Gothenburg. The T-POP will quantify for the first time the high frequency, seasonal and interannual variability of the deep Arctic Ocean temperature. This variability quantification is required for putting into context the MOSAiC and historical point measurements of the CTD. Team OCEAN had deployed two T-POPs.

Fig.5.19: Preparation of T-POP profiler before deployment.

Thermistor chain network (PI: Mario Hoppmann)

Please see Team Ice chapter.

UpTempo buoys (PI: M. Steele)

On 26 October 2019, two UpTempo thermistor chain buoys (Marlin Yug, Russia) were deployed via helicopter on sea-ice floes within the Distributed Network around 10nm west and east of *Polarstern*, respectively (Table 5.4, Figure 5.20). They were deployed as far away from each other as possible under the given circumstances, and also filling gaps within the DN with respect to ocean observations. Due to a problem with the GPS time due to a rollover software issue, a GPS drifter was deployed next to them.

Tab.5.4: Deployment info of UpTempo buoys

Deployment 1	Deployment 2
UpTempo 0930 (25m) 300234060320930	UpTempo 0940 (60m) 300234060320940

AWI-UTA-0012 (P105) 300234067707750 85°28.84' N 125°24.25' E 8:49 UTC	AWI-UTA-0009 (P102) 300234067705760 85°30.04' N 129°32.37' E 9:15 UTC

Fig.5.20: Deployment of UpTempo buoy and supplementary GPS buoy in the Distributed Network.

Snow Buoy (PI: M. Nicolaus)

On 29 October 2019, a standard Snow Buoy (MetOcean Telematics, Halifax, Canada) with the ID 2019S96 and IMEI 300234066083120 was deployed at a SYI location at the dark site. The snow heights below the four ultrasonic pingers were 0.18 m, 0.17 m, 0.14 m and 0.17 m, respectively. Deployment time and location were 1:45 UTC at 85° 38.798' N, 125° 28.241'E. The buoy was co-deployed with the SIMBA-type ice mass balance buoy PRIC 09-01 (see Team ICE chapter), and close to the deployment location of a sediment trap (see Team ECO chapter).

Aural M2 autonomous underwater hydroacoustic recorder (PI: O. Boebel)

On 29 October, an Aural M2 autonomous underwater hydroacoustic recorder (Multi electronique, Quebec, Canada) was deployed through a hydrohole at a SYI location at the dark site. The instrument was deployed at a depth of 50 m using a Kevlar rope, and was attached to two surface floats in case of ice breakup. The data is only recorded internally, and therefore a recovery before the end of the drift is mandatory.

Biogeochemical sensor package (PI: S. Torres-Valdez)

A set of biogeochemical sensors was deployed at a FYI location at the so-called "dark site", appr. 1.3 km away from *Polarstern*, on 20 November 2019. Deployment time and location were 15:00 UTC at 85° 44.817' N, 120° 14.577' E. The sensor module consisted of the following sensors, measuring a set of 11 parameters:

Tab.5.5: Sensor suite of the biogeochemical package. * denotes the ability to communicate with the respective sensor through a cable to the surface.

Sensor	Parameter
Sunburst SAMI pH*	pH

Sunburst SAMI pCO2*	CO2
Satlantic ISUS V3 + battery pack*	Nitrate
Wetlabs ECO PAR	PAR
Wetlabs ECO Triplet-W	CDOM, Chl-a, Backscatter
SeaBird SBE37-SMP-ODO*	Conductivity, Temperature, Depth, Oxygen

The sensors were fixed onto a custom-built mount (Figure 5.21), and were deployed through a hydrohole at 5.5 m depth using a Kevlar rope. Selected sensors (marked by an asterisk) were connected to data cables to the surface in order to have the ability of a regular data download. The data cables were fed through a thick rubber tube for additional protection. The installation was attached to four flotations placed on the ice surface as an emergency float in case the ice breaks up or melts. The data of most sensors is stored internally, and a recovery before the end of the drift is mandatory.

Fig.5.21: Final assembly of biogeochemical sensor package.

On 15 December 2019, the iSVP buoy 2019P154 (MetOcean Telematics, Halifax, Canada, IMEI 300234068210310, provided by PRIC) was placed next to the surface flotations as an additional means to track the sensor package in case of an ice breakup.

Preliminary (expected) results

CTD data

Data collected from CTD operation were pre-processed by using SeaBird data processing software. Different routines were used accordingly before 1 dB bin-averaged ASCII output .cnv file and .btl (bottle) file are produced. These routines are DATCNV, WILDEDIT, BOTTLE SUMMARY, SPLIT, TRANSLATE, CELL THERMAL MASS, LOOP EDIT, and BIN AVERAGE. Only downcast profiles were used to produce ASCII .cnv files, which contain both original and bin-averaged profiles. Team OCEAN submits bin-averaged .cnv files and bottle files to MCS.

Team OCEAN also provides raw .hex files and .xmlcon configuration files if participants want to process raw data by themselves.

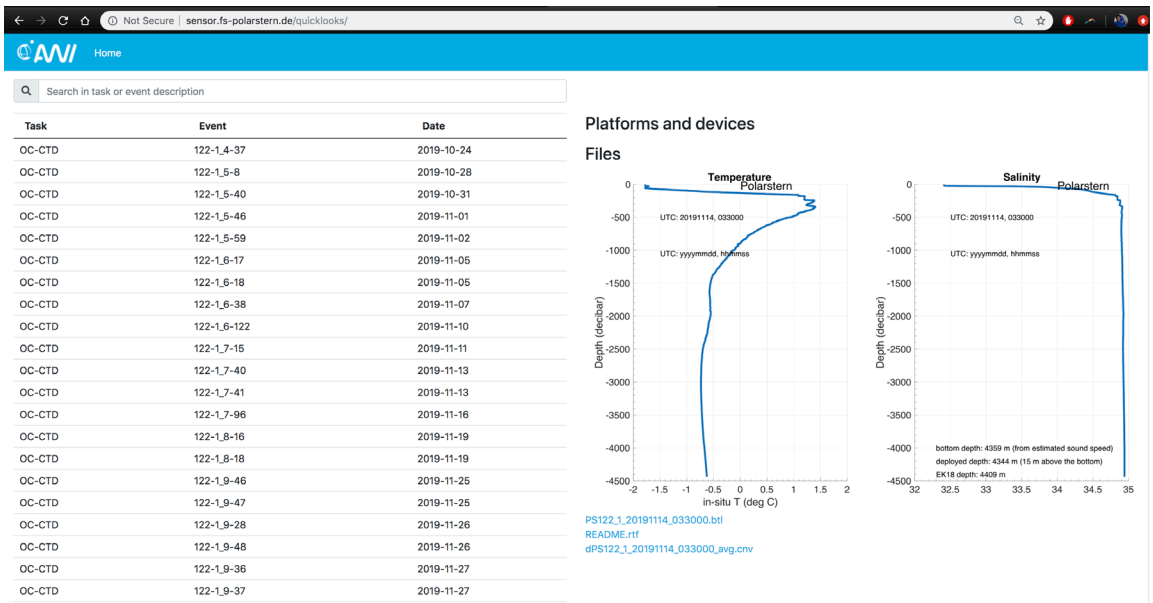

Task	Event	Date
OC-CTD	122-1_4-37	2019-10-24
OC-CTD	122-1_5-8	2019-10-28
OC-CTD	122-1_5-40	2019-10-31
OC-CTD	122-1_5-46	2019-11-01
OC-CTD	122-1_5-59	2019-11-02
OC-CTD	122-1_6-17	2019-11-05
OC-CTD	122-1_6-18	2019-11-05
OC-CTD	122-1_6-38	2019-11-07
OC-CTD	122-1_6-122	2019-11-10
OC-CTD	122-1_7-15	2019-11-11
OC-CTD	122-1_7-40	2019-11-13
OC-CTD	122-1_7-41	2019-11-13
OC-CTD	122-1_7-96	2019-11-16
OC-CTD	122-1_8-16	2019-11-19
OC-CTD	122-1_8-18	2019-11-19
OC-CTD	122-1_9-46	2019-11-25
OC-CTD	122-1_9-47	2019-11-25
OC-CTD	122-1_9-28	2019-11-26
OC-CTD	122-1_9-48	2019-11-26
OC-CTD	122-1_9-36	2019-11-27
OC-CTD	122-1_9-37	2019-11-27

Fig.5.22: A screentshot of the quicklooks page onboard. Team OCEAN provides figures and processed data here for an overview of all CTD operations.

To facilitate overview and exchange of CTD data onboard, Team OCEAN collaborated with Team DATA providing a simple figure of temperature and salinity profiles and pre-processed .cnv and .btl files to the *quicklooks* service (sensor.fs-polarstern.de/quicklooks/, Figure 5.22). We highly recommend this onboard service for colleagues in later Legs. *Quicklooks* not only saves time tracking completed CTD profiles but also gives a convenient way to share information for other teams.

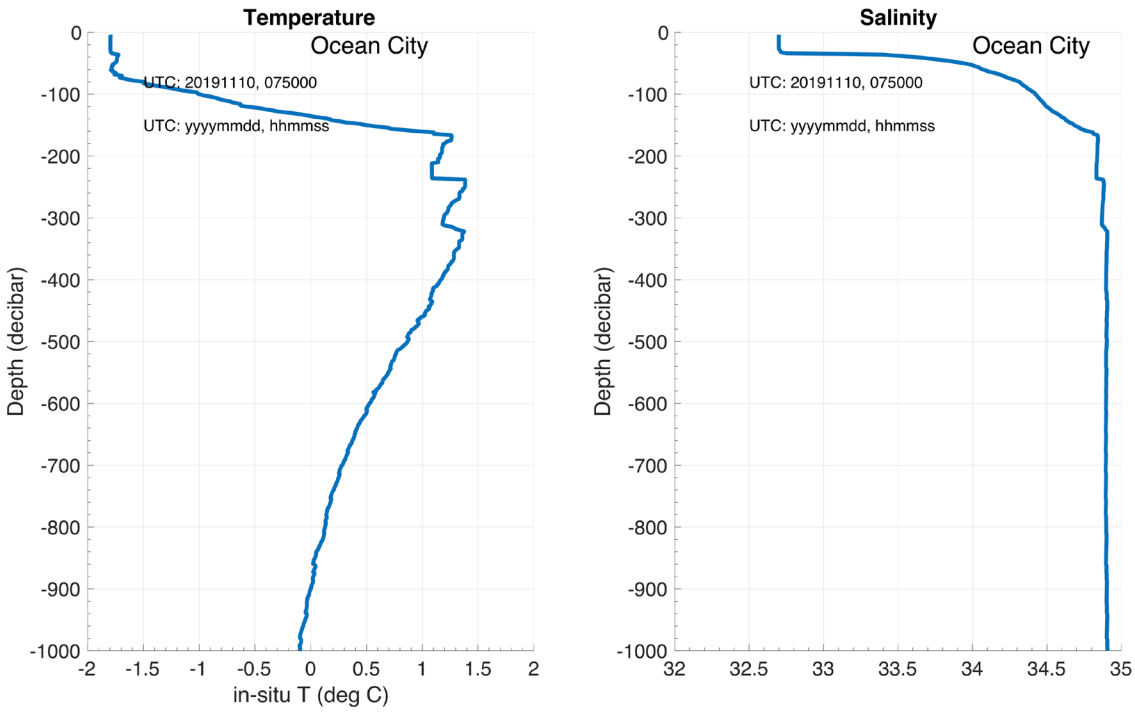

Fig.5.23: Typical CTD profile of temperature (left) and salinity (right).

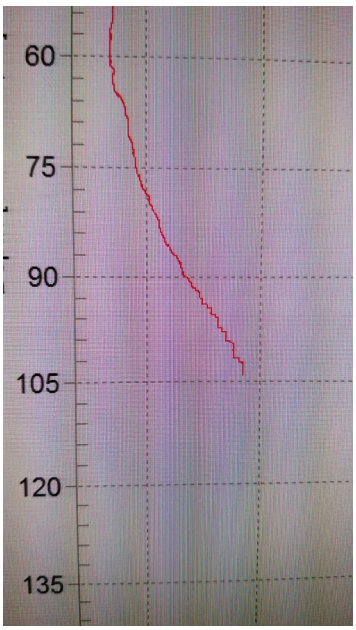

Fig.5.24: Screenshot of double diffusive staircases (see 90–105 m) during the CTD operation on 6 December.

Our drifting area is within Amundsen Basin and is partially influenced by the main stream of Atlantic waters passing Nansen Basin, which is characterized by core temperature of ~3°C and salinity of ~34.98 with ~150–400 m (Rudels et al., 2015). In the measured CTD profiles, the intrusion of Atlantic waters is usually found below ~150 m and above ~400 m (Figure 5.23). Above this Atlantic layer, a sharp thermocline (and halocline) separates the upper near-freezing (~-1.8°C) and relatively fresh (~32.7) waters. This stratification preconditions a water column which temperature and salinity have opposite effects on density (Bebieva & Timmermans, 2015) and the resultant feature is the existence of double diffusive staircases (Figure 5.24). Another type of double diffusive staircases is also seen as temperature and salinity both decrease with depths below the Atlantic layer (Figure 5.23). Sometimes they are also referred to salt fingers (Bebieva & Timmermans, 2015).

A complete perspective of the water column relies on the *Polarstern* CTD. For a ~4400-m profile (Figure 5.25), the effect of pressure becomes important below ~1000 m as the departure between the in-situ temperature and potential temperature increases with depths. The temperature profile is characterized by an intrusive Atlantic layer bounded by one upper thermocline at ~200–400 m and one lower thermocline at ~600–2000 m. Temperature below ~2000 m is less changed. On the other hand, features in the salinity profile is less pronouncing and the profile is likely a 2-layer structure with a sharp halocline at ~200 m.

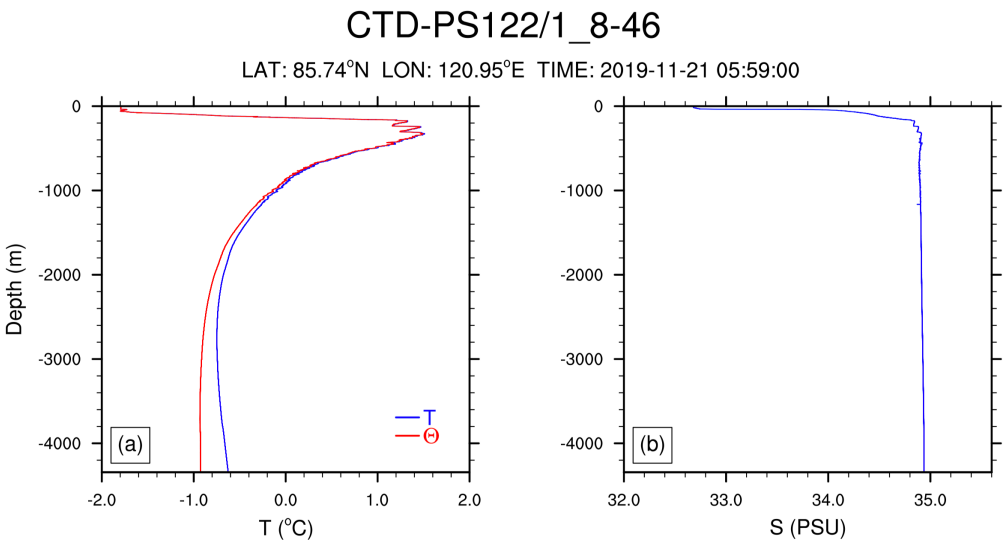

Fig.5.25: CTD profile of (a) temperature and (b) salinity taken from Polarstern on 21 November. Red line in (a) is for potential temperature and blue is for in-situ temperature.

The near-daily CTD operations provide a perfect chance to establish time series of the water column for the upper ocean. Data for the CTD profiles in November are shown together (Figures 5.26, 5.27). Although a strong wind event occurred during 16–18 November, water column below ~200 m seems to be unaffected. This is not the case, however, the upper thermocline and surface mixed layer (based on salinity here) fluctuated substantially during the course of November. The depth range of the surface mixed layer is from ~20 m to 50 m. We find that double diffusive staircases existed within the upper thermocline absent (e.g., see the profile on 19 November) after the passage of the strong wind event. Concurrently the surface mixed layer is also found deepened (Figures 5.27, 5.28) after the winds subsided. Features suggesting double diffusive staircases later reoccurred on 22 November, implying that the atmospheric forcing could transfer momentum downward the upper thermocline. Note that horizonal advection or submesoscale frontal instability could also destabilize the original stratification (e.g., Timmermans et al., 2012).

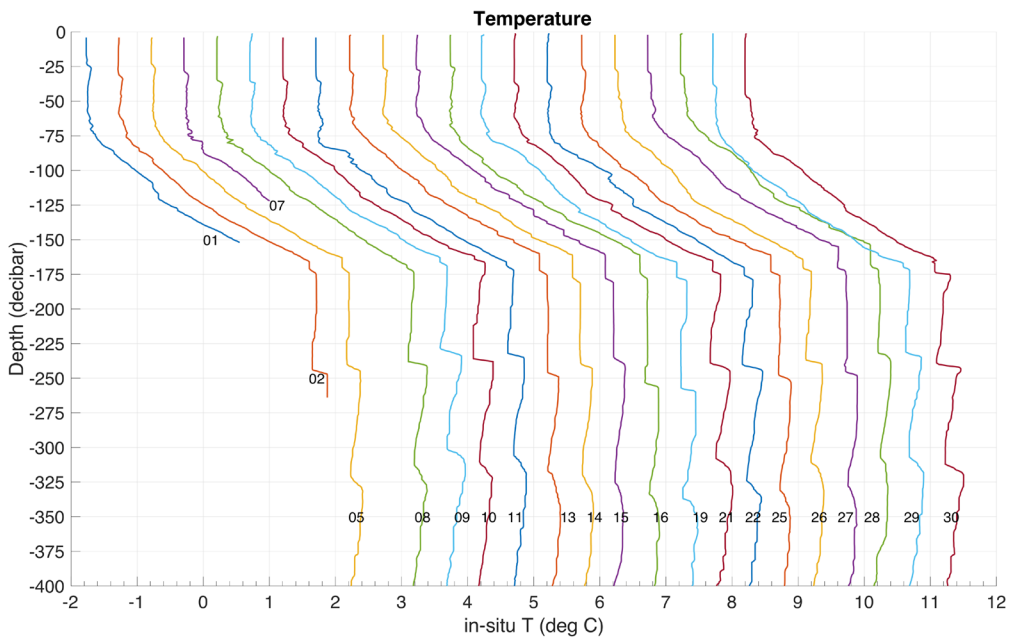

Fig.5.26: Temperature profiles made in November from both Ocean City and Polarstern CTD operations. Number indicates date of November. Each profile is offset by ~0.5℃ from the left-most profile.

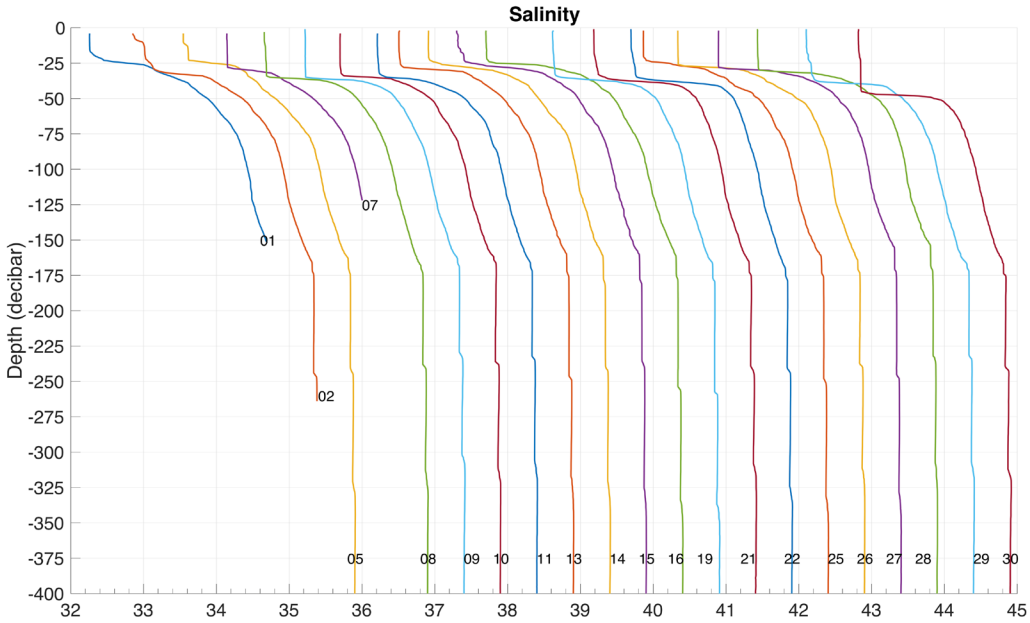

Fig.5.27: Same as Figure 5.26, but for salinity. Each profile is offset by ~0.5 from the left-most profile.

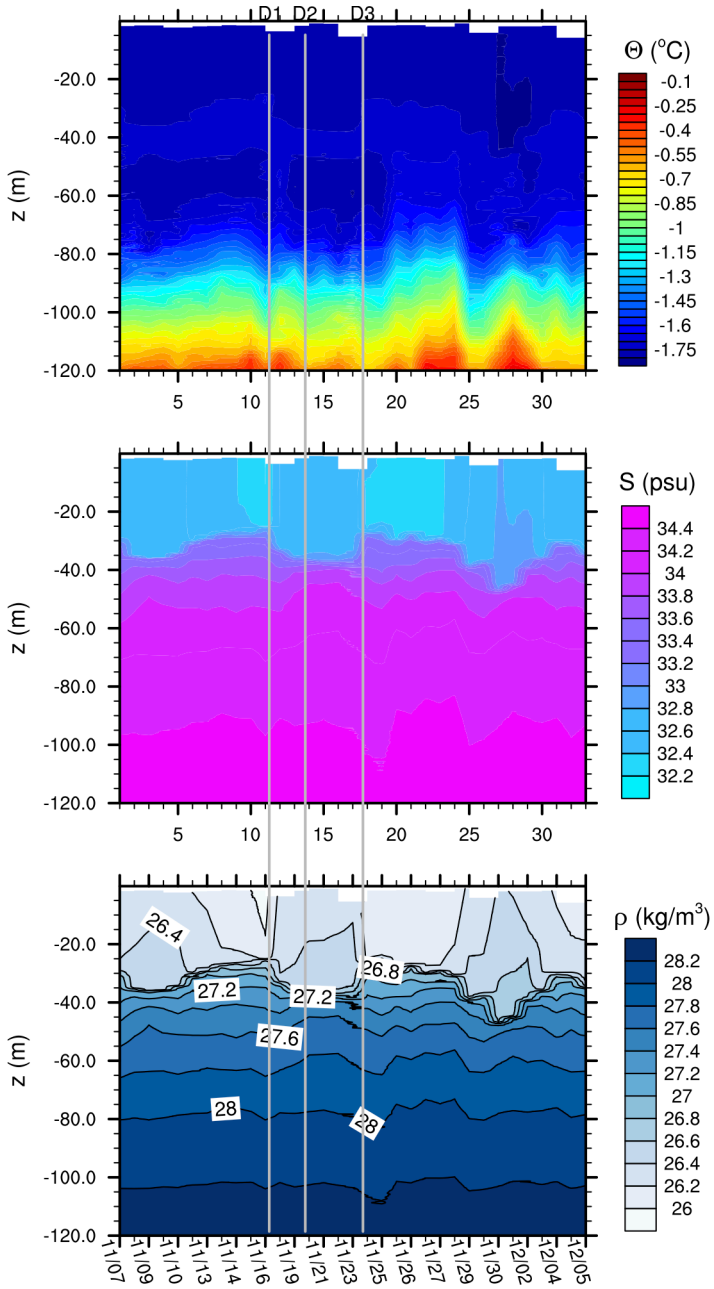

Fig.5.28: Depth-time contour of potential temperature, salinity and in-situ density from CTD profiles during 7 November–5 December. Gray lines indicate strong wind events on 17, 20, and 24 November.

Strong wind events and MSS data

There were various strong wind (>10 m s^{-1}) events in November (Figure 5.29), in which the event during 16–18 November caused an influential footprint on the main ice floe. The high wind (~20 m s^{-1}) event was resulted from a low-pressure system passing the drifting area

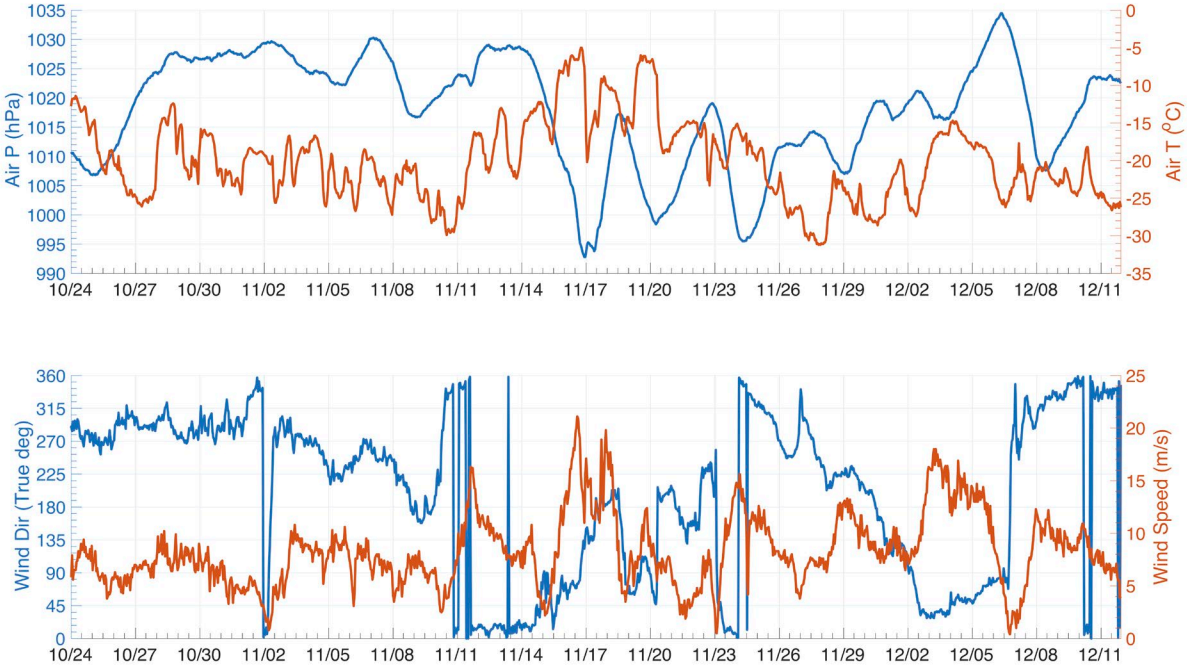

Fig.5.29: Time series of air pressure and wind direction (blue, upper and lower panels) and air temperature and wind speeds (red, upper and lower panels). Note that wind directions follow oceanographic convention that 0 degree indicates the winds blow to the north. Data are extracted from the D-Ship system on Polarstern.

Fig.5.30: Ocean City 1.0 and the newly-opened lead on 17 November. The white box on the right is the drifted-away Remote Sensing Hub.

beginning on 16 November. One day later a 20-m wide lead appeared nearby Ocean City and caused power outage for the entire main ice floe (Figure 5.30). The CTD winch in Ocean City can not be operated due to electricity shortage. Team OCEAN decided to use a generator to commence MSS profiles when it was totally blackout on the ice. Raw MSS data were preliminarily processed by using the MATLAB package developed by our turbulence team. These MSS operations were continued during the course of the wind event and the reward is

the first-hand observations (Figure 5.31) of the ice-covered upper-ocean evolution under strong winds and neighboring lead.

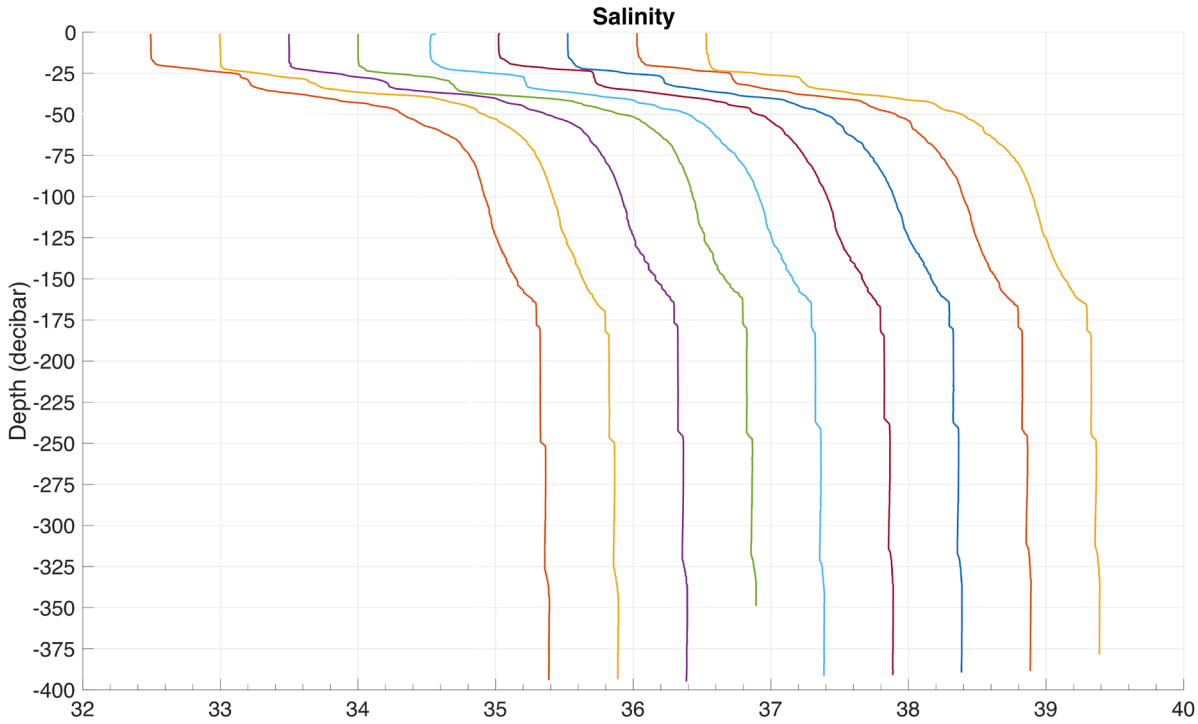

Fig.5.31: Salinity profiles made by the MSS profiler when peak winds prevailed on 17 November. Each profile is offset by ~0.5 from the left-most profile.

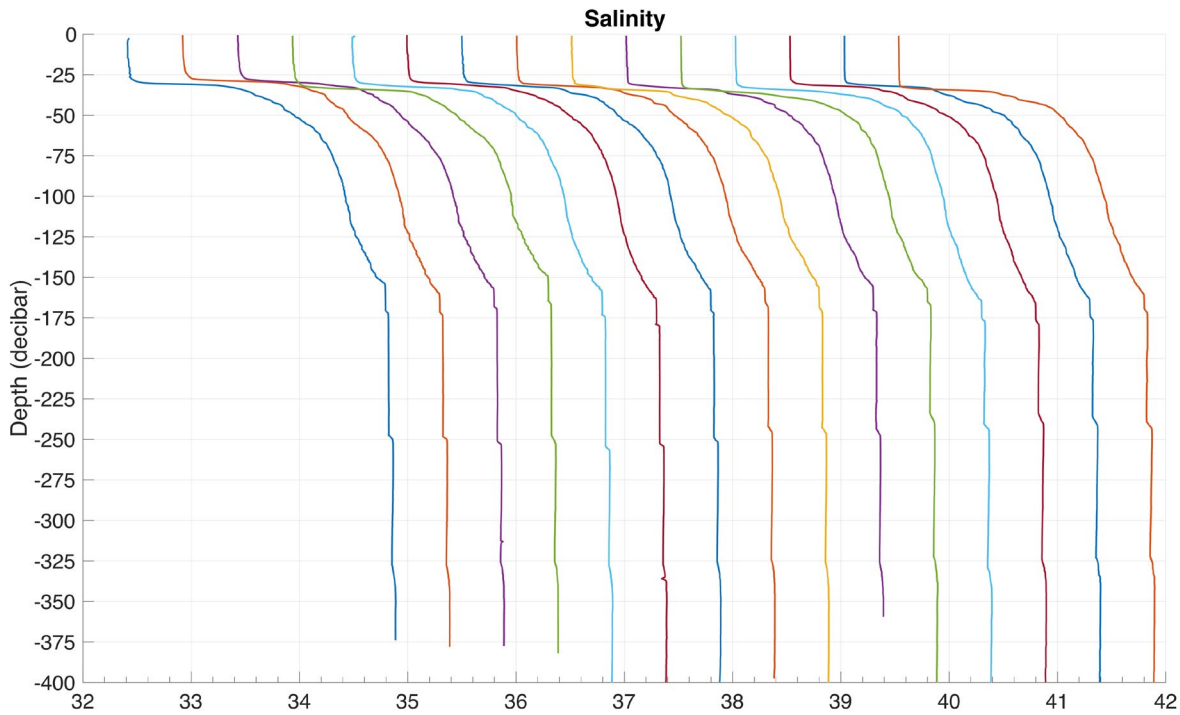

Fig.5.32: Salinity profiles made by the MSS profiler when winds subsided on 18 November. Each profile is offset by ~0.5 from the left-most profile.

It can be visualized that surface mixed layer was deepened with time on 17 November. A shallow halocline appeared at ~25 m capping a ~5 m semi-homogenous layer above the upper halocline (Figure 5.31). Note that the measurements were commenced nearby a lead which opened for ~1 day. We suspect that the thin layer below ~25 m was the old surface mixed layer that was pushed downward by the near-surface convective mixing. When we commenced further MSS profiles on 18 November then the data shows that the surface mixed layer indeed deepened for ~10 m (Figure 5.32). We believe these data would provide valuable insights on the flux exchange between the atmosphere and upper ocean, and may be useful for investigating parametrization of numerical models. Moreover, the lightweight and fast operation of the MSS profiler emphasize its value under extreme environmental conditions. In this report, we only briefly mention the collected MSS profiles during the strong wind event. Further analyses regarding turbulence and dissipation will be commenced by our turbulence research team.

Underway currents and S-ADCP data

Raw S-ADCP data is produced by the RDI vmDAS software. The raw data is synchronized every 6 hours to the Team OCEAN's public folder and is preliminarily processed by the CODAS software (http://currents.soest.hawaii.edu/docs/adcp_doc/index.html) developed by the University of Hawaii. Briefly, a virtual machine of fully configured Linux system with the CODAS software from the official CODAS website is set up in a local laptop. For monitoring the data in a daily basis, only .LTA files are processed. Further detailed post-processes regarding quality control of single ping data (.N1R and .N2R files, …etc.), are beyond the scope of on-board-processing. The post-processing will be done using the SADCP software first developed at GEOMAR Helmholtz Centre for Ocean Research Kiel with minor changes implemented at AWI.

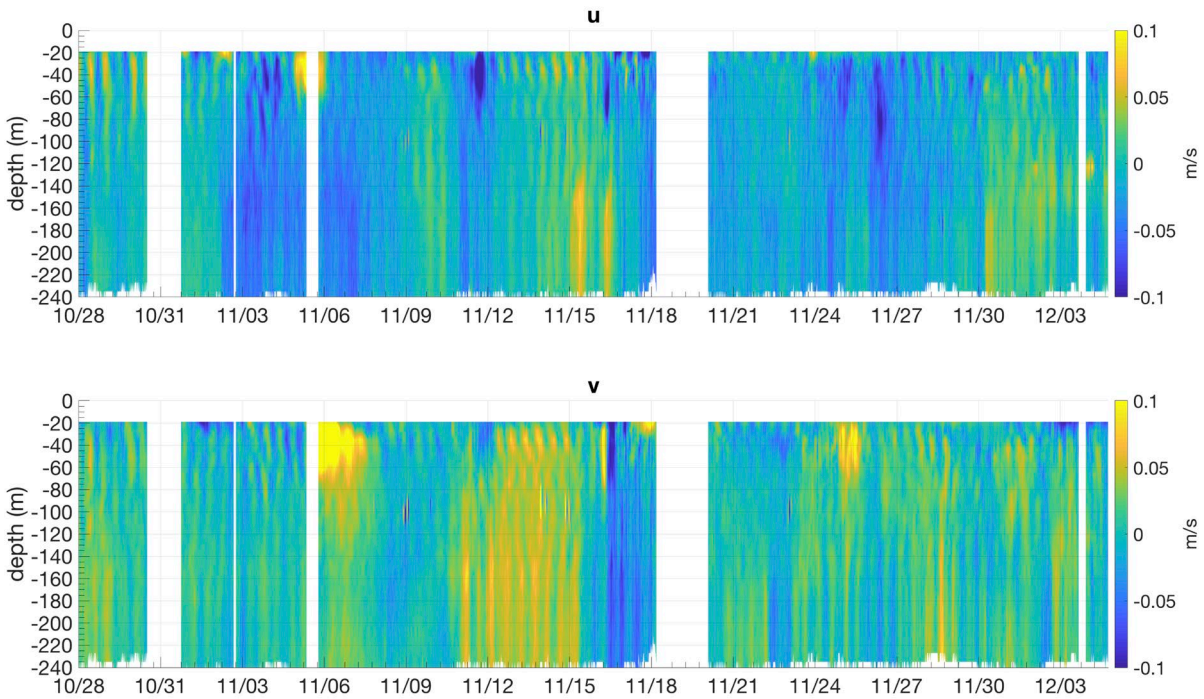

Fig.5.33: Depth-time plots of east-west (u, positive for eastward currents, upper panel) currents and north-south (v, positive for northward currents, lower panel) currents derived from S-ADCP data. Note that sporadic strong currents at ~80–100 m after 8 November indicate the interference from the Polarstern CTD.

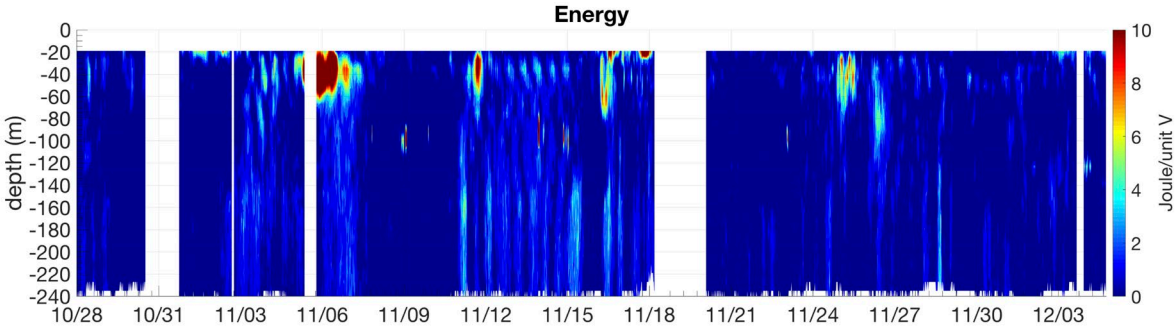

Fig.5.34: Kinetic energy of unit volume derived from the observed currents. Note that strong energy at ~80–100 m after 8 November indicate the interference from the Polarstern CTD.

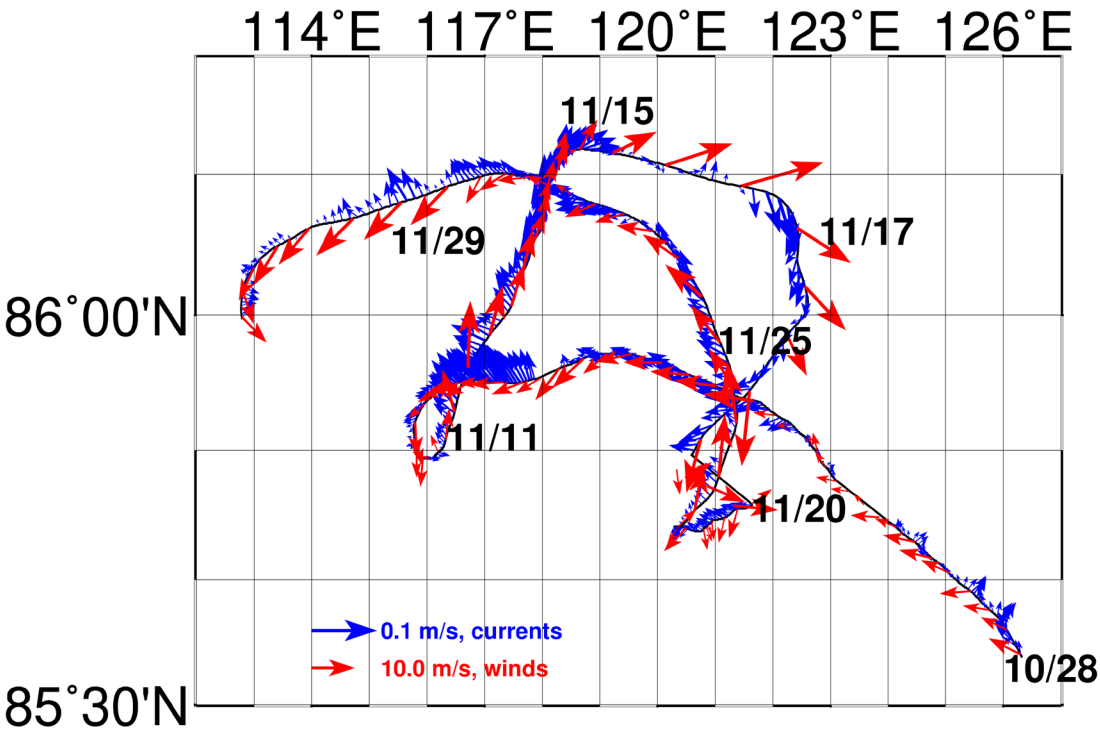

Fig.5.35: Depth-integrated currents (blue vectors) and the winds (red vectors) extracted from Polarstern in from 28 October to 1 December. Black line denotes the drifting trajectory. For clarity, vectors are subsampled.

S-ADCP data indicates that the currents during the drift were typically O(<0.1 m s^{-1}), with occasionally wind-resulted strong currents up to ~0.2 m s^{-1} in the upper ~60 m (Figure 5.33). Slanted stipes shown in the depth-time plots currents (see 12–15 and 24–30 of November) indicate the passage of surface-generated near-inertial waves (e.g., Alford et al., 2016; Halle & Pinkel, 2003). However, strong currents seen on 6 November are not clear which processes are related. A simple plot of the unit volume kinetic energy clearly shows that events and features are concentrated for the upper ~80 m (Figure 5.34). This high energy signal also coincides with the timing of the rise of strong winds (e.g., Figure 5.29), suggesting that high winds and resultant ice movements provide sources of momentum to the upper ocean. Depth-integrated currents along with the winds indicate that the upper ocean generally follow the winds (Figure 5.35). Currents tend to turn to the right-hand side of the winds, consistent to the

Ekman dynamics. More analyses are needed to interpret other small-scale features such as internal waves and (sub)mesoscale eddies.

For unknown reasons, the PC for running the vmDAS software on *Polarstern* is found that the software will get frozen. Once the software got frozen, the data acquisition stopped. This is unfortunately the case the data was not stored on 18 November so we lost an opportunity to compare both Shipboard ADCP and MSS data when the strong wind event subsided. An upgrade for the PC is recommended for future Legs.

Salinity calibrations

Water samples for salinity calibrations were proceeded for both the Ocean City and *Polarstern* CTD. Due to limited time in Ocean City, we did not collect enough water samples for salinity calibrations for the Ocean City CTD. This task will be left for later Legs.

An example of the salinity calibrations indicate that the *Polarstern* CTD has a higher reading than that given by the OPS salinometer (Figure 5.36). Aggregate the water samples for salinity calibrations for the *Polarstern* CTD, the overall mean bias (standard deviation) of the primary conductivity sensor is 0.00500 (0.00106), showing slightly better performance than the secondary conductivity sensor (Figure 5.37). Based on these results, we recommend to subtract a mean salinity bias of ~0.005 from the salinity measurements of the primary and secondary conductivity sensors, respectively. Overall, the root-mean-squared errors of the measured salinities from the two conductivity sensors are ~0.005. Final calibration will be done according to the standard CTD-calibration performed at AWI.

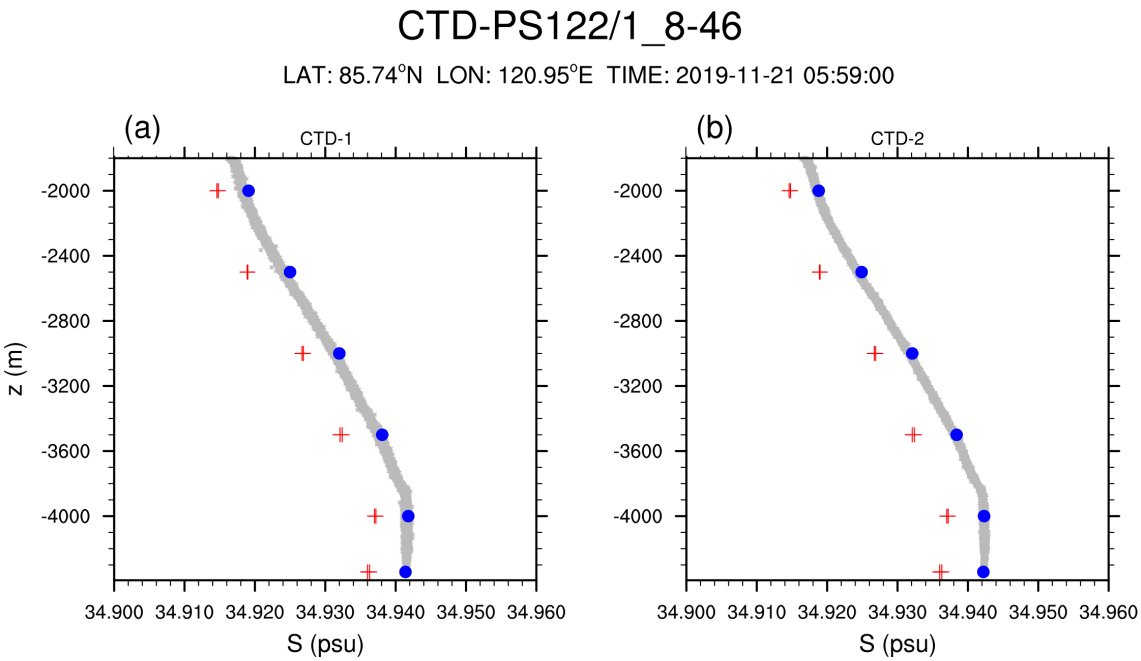

Fig.5.36: Salinity comparisons among OPS salinometer (red cross), downcast profile (gray line), and collected water samplers (blue dots). Data is from the CTD operation on Polarstern on 21 November. (a) is for the primary conductivity sensor and (b) is for the secondary conductivity sensor.

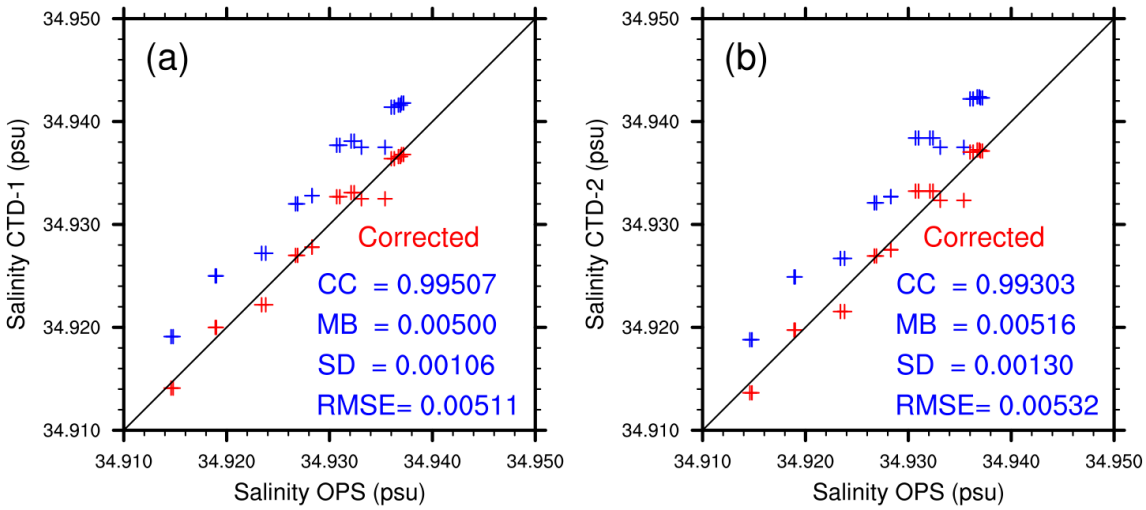

Fig.5.37: Statistics of correlation coefficients (CC), mean biases (MB), standard deviations (SD), and root-mean-square error (RMSE) of comparisons between salinities derived the Polarstern CTD and OPS salinometer. Blue crosses indicate salinities before correction, while red crosses denote corrected salinities by subtracting a mean bias. (a) is for the primary conductivity sensor and (b) is for the secondary conductivity sensor.

SIT buoy data from M-sites in the Distributed Network

Since the first deployment of the M sites on 2 October, we are able to track those autonomous Salinity Ice Tether (SIT, see the Distributed Network cruise report) buoys from Bremerhaven. Unfortunately, three out of the eight buoys were likely failed after 13 November due to deformed ice ridge or unknown technical issues. Based on the received trajectories it suggests that the ice field around the main ice floe moves coherently with each other (Figure 5.38). Each of the trajectories seems to follow the main ice floe but with an offset. This provides valuable information regarding the stability and convergence/divergence of the ice field.

Examining the time series from one of the buoys, SIT #1, we find the data suggesting two important features in the first half of November (Figure 5.39). First, the temperatures at ~50 m can be decreased to the freezing temperatures, suggesting the deepening of the surface mixed layer. Meanwhile the temperatures at ~100 m fluctuate significantly compared to the shallower depths. We suspect there exists multiple internal wave packets by visual inspection of the time series. Second, the stratification in terms of the vertical gradient of salinity is still very strong (~0.04 m^{-1}), comparing with salinities from 20 and 50 m. This contradicts the scenario suggested by the temperature time series, thus lateral advection of cold waters from elsewhere could account for the observed signal. Interestingly we also observe the rise of salinities at ~20 m on 16–17 November, indicating ice formation during the lead event. This is consistent to the MSS data and further support our argument that convective mixing is important during the strong wind event.

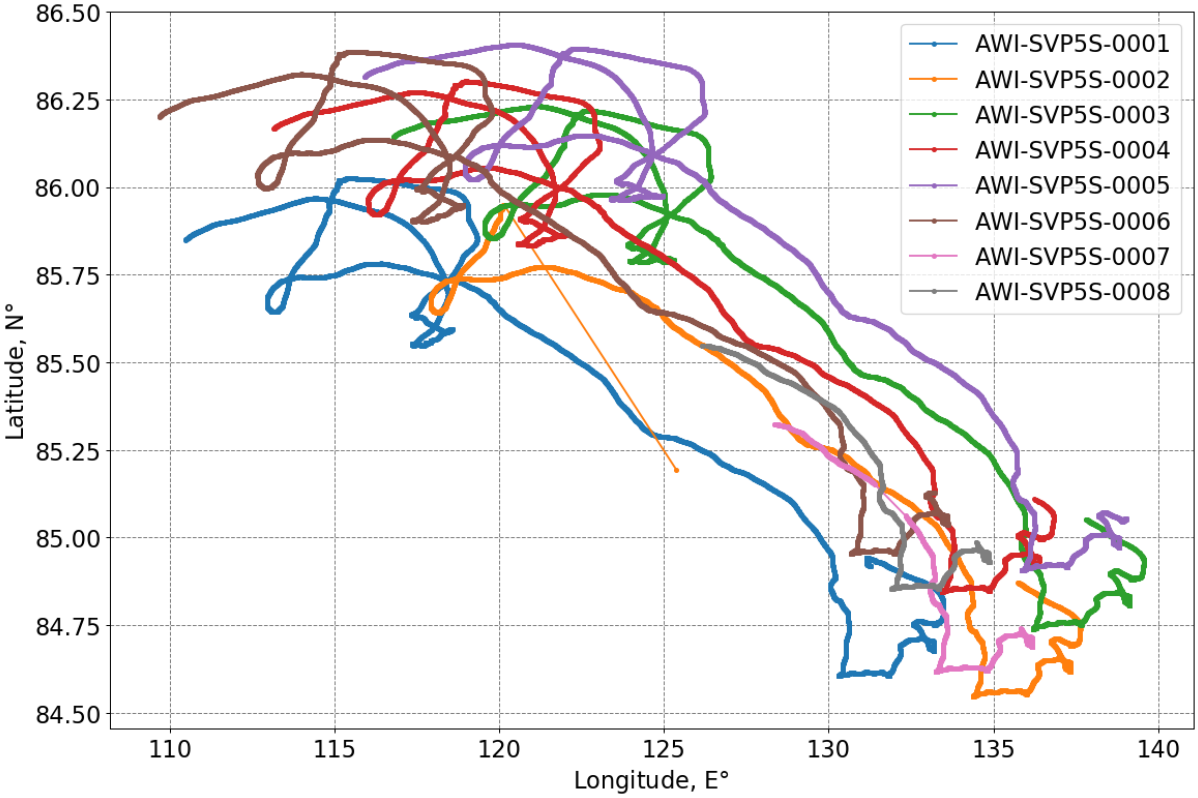

Fig.5.38: Drifting trajectories of the eight SIT buoys (from Ivan Kuznetsov).

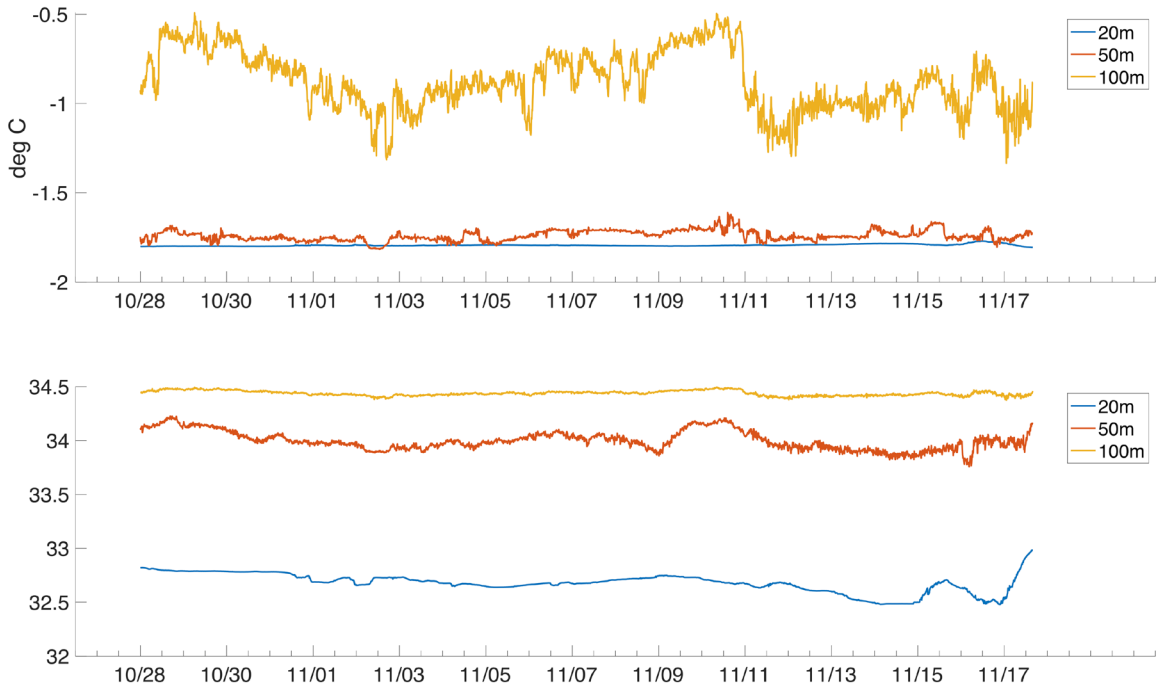

Fig.5.39: Time series of temperatures (upper panel) and salinities (lower panel). Blue, red, and yellow lines indicate measurements at 20, 50, and 100 m, respectively.

Data management

All data are handled, documented, archived and published following the MOSAiC data policy (see APPENDIX). Final data products will be stored at the PANGAEA data repository (World Data Center PANGAEA Data Publisher for Earth & Environmental Science (www.pangaea.de)).

References

Alford MH, MacKinnon JA, Simmons HL & Nash JD (2016) Near-Inertial Internal Gravity Waves in the Ocean. Annual Review of Marine Science, 8, 95–123. https://doi.org/10.1146/annurev-marine-010814-015746

Bebieva Y, Timmermans ML (2015) An examination of double-diffusive processes in a mesoscale eddy in the Arctic Ocean. Journal of Geophysical Research: Oceans, 121(1), 457–475. https://doi.org/doi:10.1002/2015JC011105

D'Asaro EA, Morehead MD (1991) Internal waves and velocity fine structure in the Arctic Ocean. Journal of Geophysical Research: Oceans, 96(C7), 12725–12738. https://doi.org/10.1029/91JC01071

Guthrie JD, Morison JH, Fer I (2013) Revisiting internal waves and mixing in the Arctic Ocean. Journal of Geophysical Research: Oceans, 118(8), 3966–3977. https://doi.org/10.1002/jgrc.20294

Halle C, Pinkel R (2003) Internal wave variability in the Beaufort Sea during the winter of 1993/1994. Journal of Geophysical Research: Oceans, 108(C7), n/a-n/a. https://doi.org/10.1029/2000JC000703

Manucharyan GE, Thompson AF (2017) Submesoscale Sea Ice-Ocean Interactions in Marginal Ice Zones. Journal of Geophysical Research: Oceans, 122(12), 9455–9475. https://doi.org/10.1002/2017JC012895

Morison JH, Long CE, Levine MD (1985) Internal wave dissipation under sea ice. Journal of Geophysical Research: Oceans, 90(C6), 11959–11966. https://doi.org/10.1029/JC090iC06p11959

Polyakov IV, Pnyushkov AV, Rember R, Ivanov VV, Lenn YD, Padman L, Carmack EC (2012) Mooring-Based Observations of Double-Diffusive Staircases over the Laptev Sea Slope*. Journal of Physical Oceanography, 42(1), 95–109. https://doi.org/10.1175/2011JPO4606.1

Polyakov IV, Pnyushkov AV, Alkire MB, Ashik IM, Baumann TM, Carmack EC et al. (2017) Greater role for Atlantic inflows on sea-ice loss in the Eurasian Basin of the Arctic Ocean. Science, 356(6335), 285–291. https://doi.org/10.1126/science.aai8204

Proshutinsky AY, Johnson MA (1997) Two circulation regimes of the wind-driven Arctic Ocean. Journal of Geophysical Research: Oceans, 102(C6), 12493–12514. https://doi.org/doi:10.1029/97JC00738

Rabe, B, Heuzé, C, Regnery, J, Aksenov, Y, Allerholt, J, Athanase, M, Bai, Y, Basque, C, Bauch, D, Baumann, TM, Chen, D, Cole, ST, Craw, L, Davies, A, Damm, E, Dethloff, K, Divine, DV, Doglioni, F, Ebert, F, Fang, Y-C, Fer, I, Fong, AA, Gradinger, R, Granskog, MA, Graupner, R, Haas, C, He, H, He, Y, Hoppmann, M, Janout, M, Kadko, D, Kanzow, T, Karam, S, Kawaguchi, Y, Koenig, Z, Kong, B, Krishfield, RA, Krumpen, T, Kuhlmey, D, Kuznetsov, I, Lan, M, Laukert, G, Lei, R, Li, T, Torres-Valdés, S, Lin, L, Lin, L, Liu, H, Liu, N, Loose, B, Ma, X, MacKay, R, Mallet, M, Mallett, RDC, Maslowski, W, Mertens, C, Mohrholz, V, Muilwijk, M, Nicolaus, M, O'Brien, JK, Perovich, D, Ren, J, Rex, M, Ribeiro, N, Rinke, A, Schaffer, J, Schuffenhauer, I, Schulz, K, Shupe, MD, Shaw, W, Sokolov, V, Sommerfeld, A, Spreen, G, Stanton, T, Stephens, M, Su, J, Sukhikh, N, Sundfjord, A, Thomisch, K, Tippenhauer, S, Toole, JM, Vredenborg, M, Walter, M, Wang, H, Wang, L, Wang, Y, Wendisch, M, Zhao, J, Zhou, M, Zhu, J. 2022. Overview of the MOSAiC expedition: Physical oceanography. *Elementa: Science of the Anthropocene* 10(1). DOI: https://doi.org/10.1525/elementa.2021.00062

Rudels B, Schauer U, Björk G, Korhonen M, Pisarev S, Rabe B, Wisotzki A (2013) Observations of water masses and circulation with focus on the Eurasian Basin of the Arctic Ocean from the 1990s to the late 2000s. Ocean Science, 9(1), 147–169. https://doi.org/10.5194/os-9-147-2013

Rudels B, Korhonen M, Schauer U, Pisarev S, Rabe B, Wisotzki A (2015) Circulation and transformation of Atlantic water in the Eurasian Basin and the contribution of the Fram Strait inflow branch to the Arctic Ocean heat budget. Progress in Oceanography, 132, 128–152. https://doi.org/10.1016/j.pocean.2014.04.003

Timmermans ML, Proshutinsky A, Krishfield RA, Perovich DK, Richter-Menge JA, Stanton TP, Toole JM (2011) Surface freshening in the Arctic Ocean's Eurasian Basin: An apparent consequence of

recent change in the wind-driven circulation. Journal of Geophysical Research: Oceans, 116(C8). https://doi.org/doi:10.1029/2011JC006975

Timmermans ML, Cole S, Toole J (2012) Horizontal Density Structure and Restratification of the Arctic Ocean Surface Layer. Journal of Physical Oceanography, 42(4), 659–668. https://doi.org/10.1175/JPO-D-11-0125.1